Instrumentation for hydrogenative parahydrogen-based hyperpolarization techniques

(Article begins on next page)

Instrumentation for Hydrogenative Parahydrogen-Based Hyperpolarization Techniques

Andreas B. Schmidt,[1,2] C. Russell Bowers,[3,4] Kai Buckenmaier,[5] Eduard Y. Chekmenev,[6,7] Henri de Maissin,[1,2] James Eills,[8,9] Frowin Ellermann,[10] Stefan Glöggler,[11,12] Jeremy W. Gordon,[13] Stephan Knecht,[14] Igor V. Koptyug,[15] Jule Kuhn,[10] Andrey N. Pravdivtsev,[10] Francesca Reineri,[16] Thomas Theis,[17] Kolja Them,[10] and Jan-Bernd Hövener[10]

1 Department of Radiology – Medical Physics, Medical Center, University of Freiburg, Faculty of Medicine, University of Freiburg, Killianstr. 5a, Freiburg 79106, Germany

2 German Cancer Consortium (DKTK), partner site Freiburg and German Cancer Research Center (DKFZ), Im Neuenheimer Feld 280, Heidelberg 69120, Germany

3 Department of Chemistry, University of Florida, 2001 Museum Road, Gainesville, Florida 32611, USA

4 National High Magnetic Field Laboratory, 1800 E. Paul Dirac Drive, Tallahassee, Florida 32310, USA

5 High-Field Magnetic Resonance Center, Max Planck Institute for Biological Cybernetics, Max-Planck-Ring 11, 72076, Tübingen, Germany

6 Intergrative Biosciences (Ibio), Department of Chemistry, Karmanos Cancer Institute (KCI), Wayne State University, 5101 Cass Ave, Detroit, MI 48202, United States

7 Russian Academy of Sciences (RAS), Leninskiy Prospect, 14, 119991 Moscow, Russia

8 Institute for Physics, Johannes Gutenberg University, D-55090 Mainz, Germany

9 GSI Helmholtzzentrum für Schwerionenforschung GmbH, Helmholtz-Institut Mainz, 55128 Mainz, Germany

10 Section Biomedical Imaging, Molecular Imaging North Competence Center (MOIN CC), Department of Radiology and Neuroradiology, University Medical Center Kiel, Kiel University, Am Botanischen Garten 14, 24118, Kiel, Germany

11 NMR Signal Enhancement Group Max Planck Institutefor Biophysical Chemistry Am Fassberg 11, 37077 Göttingen, Germany

12 Center for Biostructural Imaging of Neurodegeneration of UMG Von-Siebold-Str. 3A, 37075 Göttingen, Germany

13 Department of Radiology & Biomedical Imaging, University of California San Francisco, 185 Berry St., San Francisco, CA, 94158, USA

14 NVision Imaging Technologies GmbH, 89081 Ulm, Germany

15 International Tomography Center, SB RAS, 3A Institutskaya St., Novosibirsk 630090, Russia

16 Dept. Molecular Biotechnology and Health Sciences, Via Nizza 52, University of Torino, Italy

17 Departments of Chemistry, Physics and Biomedical Engineering, North Carolina State University, Raleigh, NC, 27695, USA

CONTENTS

INTRODUCTION

The unique properties of the entangled, antisymmetric nuclear spin state of dihydrogen, *para*-hydrogen (pH$_2$), has intrigued physicists, chemists, and other scientists for almost a century. pH$_2$ was used as a model system in the early days of quantum mechanics[1] and is used for fueling rockets as well as combustion-free cars today. In the 1980s, pH$_2$ was discovered as a convenient and potent source of spin order, allowing the enhancement of the signals of magnetic resonance (MR) by several orders of magnitude.[2–4] In the advent of hyperpolarized (HP) contrast agents (CA) for biomedical MR imaging (MRI) that followed, pH$_2$-based hyperpolarization methods played an important role in the acquisition of the first HP ^{13}C *in vivo* images (Fig. 1).[5,6]

Ever since, pH$_2$ has proven to be highly valuable for analytical investigations and fundamental research, *e.g.*, in analytical and catalytic chemistry or in the physics of singlet spin states.[7–10]

pH$_2$ is produced fast and stored easily. As one of four (nuclear) spin states of dihydrogen, 25 % of H$_2$ at room temperature are pH$_2$, while the other 75 % are *ortho*-Hydrogen (oH$_2$, following the Boltzmann distribution). At lower temperatures, however, the para-fraction becomes more and more enriched until at approx. 25 K, 100 % pH$_2$ is obtained. While the para-enrichment is fast using appropriate catalyst, pH$_2$ can be stored for hours to days at room temperature without significant loss if the catalyst is absent. These unique properties make pH$_2$ a spin order that can be produced easily, stored conveniently (in a pressurized bottle) and used on demand, *e.g.*, for producing hyperpolarized CAs or observing chemical reactions with enhanced sensitivity.

When it comes to clinical applications, however, dissolution dynamic nuclear polarization (dDNP) evolved faster than pH$_2$–based HP methods.[11,12] The reasons for this may be that a) at first, only few biologically relevant CAs were available (because of limited chemistry at that time), b) that mastering the complex process of pH$_2$ induced polarization (PHIP) was not straight forward (involving quantum mechanics, chemical reactions, and magnetic resonance tailored to each individual CA) and that c), no pH$_2$-polarizers were commercially available, while there were at least three different generations for dDNP.
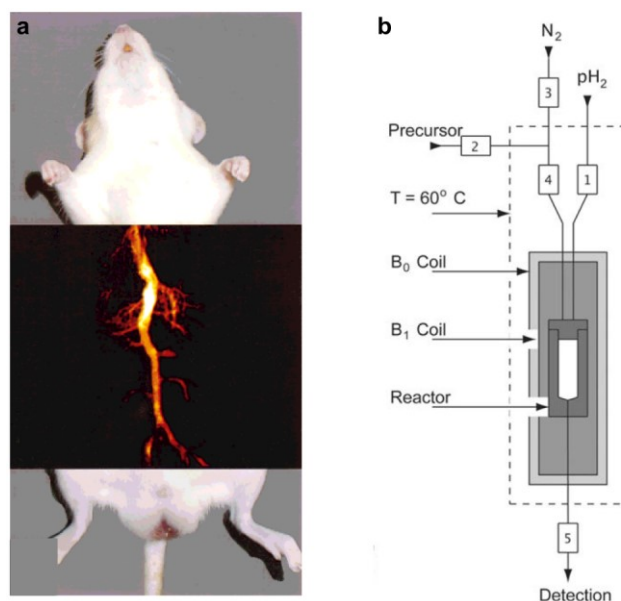
Figure 1. First hyperpolarized ^{13}C *in vivo* MRI ever published (a). The contrast agent, hydroxyethyl [1-^{13}C]propionate-d$_3$ (HEP), was produced using a prototype commercial millitesla polarizer (Amersham Biosciences, healthcare company), similar to the one shown schematically in (b). Broadly speaking, the polarizers consisted of a unit handling the fluids, the actual hyperpolarization (spin-order transfer), and the coordination of the entire process (numbers 1 – 5 represent valves). Images reproduced from Parahydrogen-Induced Polarization in Imaging: Subsecond 13C Angiography, Golman, K.; Axelsson, O.; Johannesson, H.; Mansson, S.; Olofsson, C.; Petersson, J. S. Magn. Reson. Med., Vol. 46, Issue 1 (ref 5). Copyright 2001 Wiley (a), and reprinted by permission from Springer: Magn Reson Mater Phy, PASADENA Hyperpolarization of 13C Biomolecules:

Equipment Design and Installation, Hövener, J.-B.; Chekmenev, E. Y.; Harris, K. C.; Perman, W. H.; Robertson, L. W.; Ross, B. D.; Bhattacharya, P., Vol. 22 (ref 13). Copyright Springer 2009. (b).

While pH$_2$ is easily produced in large quantities, at low cost and with a shelf life of days (depending on the storing conditions), there are some hurdles to overcome before a CA is ready for administration. For one, the pH$_2$ spin order *per se* is MR invisible (total spin of 0!) and well hidden inside the dihydrogen molecule. To obtain a hyperpolarized CA from pH$_2$, typically, the following steps have to be taken: a), bringing pH$_2$ and the target into contact (by catalytic addition or reversible exchange); b), to transfer or transform the pH$_2$-derived spin order into a desired form; and c), the purification and quality assurance (QA) prior to an *in vivo* application.

These steps usually involve a chemical reaction at elevated temperatures, pressures, sometimes in aggressive media or extreme pH – synchronized with quantum mechanical spin order transfer (SOT) mediated by evolution at constant or varying magnetic fields and radiofrequency (RF) pulses. To realize this process, various devices have been ingeniously devised; however, a single, unified design has not yet emerged. The lack of such a device may be attributed to the fact that the power and versatility of pH$_2$ has resulted in quite a few different methods – the magnetic fields alone vary by a factor of 10^9 (from nanotesla to tesla). Even today, pH$_2$ hyperpolarization methods keep evolving at a fast pace; among the ground-breaking advances, SABRE,[14] gases,[15,16] continuos HP,[17–19] PHIP-SAH,[20] RASER,[21–23] precipitation,[24] and relay methods[25,26] are only examples from the last decade. These methods require specific experimental conditions and ultimately dedicated instrumentation, which differs from method to method.

For a standardized, clinical application of a specific contrast agent, however, a consolidated setup is required, that can be certified and approved, provides reliable polarization and quality assurance. In this respect, much can be learned from SEOP[27] and DNP[11,12] with respect to polarizers and regulatory approval.

Here, we review the different instrumentations for pH$_2$ hyperpolarization, with an emphasis on biomedical application. To keep this review concise, we focus on setups for hydrogenative pH$_2$-based hyperpolarization alone and the most recent literature (~last 5 years); still, we refer to pioneering and game-changing developments whenever appropriate, and when other methods (SABRE, DNP, SEOP, *etc.*) show similar instrumentational aspects. Dedicated reviews on SABRE-related instrumentation, spin-order transfer, and pH$_2$ production are expected to be published elsewhere.

ANALYSIS OF PH$_2$ POLARIZERS

The requirements for a biomedical polarizer may be defined as to i) provide a clean, ii) aqueous solution of iii) highly polarized, iv) appropriately concentrated agents at v) physiological conditions that is preferably produced in a iv) good-manufacturing process (GMP). To make such a contrast agent, the role of hardware may be categorized as follows:

1. making the pH$_2$ spin order available to the target molecule (hydrogenation);
2. transferring the pH$_2$-derived spin order into the desired spin hyperpolarization (typically longitudinal X-nuclear magnetization);
3. purification of the solution and assuring quality.

We will elaborate on these steps in the following.

Parahydrogen addition

Before the addition, the lifetime of gaseous[28–30] or dissolved[31–33] pH$_2$ is typically long (days or many minutes, respectively). However, once bound to the catalyst[34] or the precursor,[9,35–39] the lifetime of the spin order is drastically reduced because the added protons, referred to as I$_1$ and I$_2$, interact with the environment and the rest of the (now larger) spin system. Thus, the hydrogenation should be conducted as fast as possible to reduce relaxation losses. The hydrogenation kinetics are typically affected by a multitude of coupled reaction parameters, like temperature, pH$_2$-availability, solvent, catalyst, precursor molecule or pH value. While the catalyst is needed for the addition, it may cause relaxation at the same time and needs to be removed before an injection if it is harmful.

The starting point for the SOT, *i.e.* the density matrix after the hydrogenation, is strongly dependent on the coupling between I$_1$ and I$_2$. It is determined by the molecular structure and the external static magnetic field B_0. If the spins are "strongly coupled" (that is, if their mutual J-coupling J_{I1I2} is much larger than the difference of their Larmor precession frequencies δv ($\delta v \ll J_{I1I2}$)), the eigenstates of the two-spin system are essentially the singlet-triplet (S-T) basis states. In this case, the "singlet spin order" $\mathbf{I_1 \cdot I_2} = I_{1x}I_{2x} + I_{1y}I_{2y} + I_{1z}I_{2z}$ (also known as J-order) is usually the starting point for the SOT. In the opposite case ($\delta v \gg J_{I1I2}$), the spins are referred to as weakly coupled. Then, $I_{1z}I_{2z}$ spin order is typically the starting point for SOT after the off-diagonal elements of the density matrix were averaged away during the hydrogenation.[40] However, $\mathbf{I_1 \cdot I_2}$ order can be preserved in weakly coupled systems by applying sufficiently strong ^{1}H decoupling,[41,42] or can be encountered in effectively instantaneous reactions as in photo-PHIP experiments,[43,44] where reactions with pH$_2$ happen within a few microseconds.

The exact form of the spin order in the intermediate coupling regime, including the effect from singlet-triplet (S-T) mixing at the hydrogenation catalysts, was described by Bowers, Natterer and others.[39,45–48] Such S-T mixing takes place in high and low fields and is one of the main reasons for reduced hyperpolarization yield.

In so-called PASADENA experiments (pH$_2$ and synthesis allows dramatically enhanced nuclear alignment), hydrogenation and SOT (or direct proton detection) take place at the same magnetic field.[3] Another experimental scheme often applied is referred to as ALTADENA (adiabatic longitudinal transport after dissociation engenders net alignment).[49] The latter typically features hydrogenation at lower fields (with S-T eigenbasis) followed by an adiabatic (slow) increase of B_0 into the weakly-coupled regime.[50] This results in population of either the $|\alpha\beta\rangle$ or the $|\beta\alpha\rangle$ state of the high-field Zeeman eigenbasis, where α is the spin up, and β is

the spin down state in the combined spin angular momentum state of both nuclei.

Spin-order transfer

As the literature on SOT may fill an entire review article alone,[51] we are focusing on the parts relevant for the instrumentation only.

The available spin order after hydrogenation, the spin system, its eigenstates and its interactions determine the most-effective SOT strategy. While the molecular spin system as such is usually fixed (with workarounds, *e.g.* PHIP-SAH,[20] PHIP-X[26]), the interactions can be tailored to some extent by varying the (static) external magnetic field (B_{SOT}) or by applying B_1 fields over a period of time.[52] Likewise, the spin system can be affected, to some degree, by isotope labeling and reaction parameters such as temperature and pH. Deuteration is a convenient way to reduce relaxation and simplify the spin system, *e.g.*, to an effective 3-spin-½ system in RF-pulsed SOT.[42,53,54]

Roughly speaking, a SOT can be achieved by:

- Evolution at one static field (sometimes referred to as "spontaneous" transfer),
- Evolution at different fields – magnetic field cycling (MFC-SOT)[20,24,55,56],
- Evolution plus specific manipulations by RF pulses (RF-SOT)[9,40,42,51,57–64].

Understanding the SOT requires profound knowledge of the underlying quantum mechanics. While analytical equations can be derived for simple systems, numerical simulations are usually required to determine the optimal parameters of more complex or realistic systems. These simulations can be implemented in any programming environment capable of matrix algebra. Using or building on existing (open source) packages may be convenient.[65–68]

Realizing the different variants of SOT usually requires a magnet (superconducting, resistive, permanent; sometimes shims), sometimes a multi-layer mu-metal shield (to reach fields B_{SOT} in the nanotesla or microtesla range), and an NMR unit to excite and receive MR signal.

Purification and Quality Assurance

While the addition of pH$_2$ is performed by catalysis at sometimes harsh conditions, a physiological solution devoid of the catalyst is needed for *in vivo* administration. Various approaches have been described to achieve this goal, including:

- Filtering homogeneous catalysts,[69]
- Using immobilized catalysts that remain in the polarizer,[70–72]
- Heterogeneous catalysts that facilitate filtration,[18,71,73–78]
- Phase separation and precipitation.[24,79–82]

Different agents will generally require individual approaches as their chemical properties vary significantly. A QA module similar to that used for DNP will have to encompass (at least) purity, pH, a low bioburden and temperature; no such device has emerged yet. For all approaches, time is of the essence, as

precious signal enhancement is rapidly lost once the agent is hyperpolarized.

Components and capabilities of a polarizer

Orchestrating these steps requires a dedicated unit, often referred to as a "polarizer". Some have been described, with varying goals, properties, and capabilities, *e.g.*, SOT schemes, pressures, temperatures, *in situ* detection, automation, dosing, *etc*.[13,24,36,38,42,55,83–90] For convenience, such a polarizer may be separated in different units, some of which were described in literature:

- A fluid unit, handling the gases and liquids. It is typically composed of electromagnetic, manual, or pneumatic valves and tubes, borrowed, *e.g.*, from high performance liquid chromatography (HPLC), as well as a custom-made reaction chamber or a (high-pressure) NMR tube. Inert materials, pressure and temperature resistance are important factors, as is the option to clean or sterilize.[91]
- An NMR unit, taking care of the SOT either by applying a constant magnetic field, a defined field cycle, or RF pulses. Low-field detection facilitates flip angle calibration and quality assurance.[91–93]
- A control unit: a software controlling a digital-to-analog converter (DAC) and an analog-to-digital converter (ADC), *e.g.*, for switching valves, B_0 control, temperature readings, NMR. These needs have been addressed by using the hardware of the NMR / MRI,[87,88,94] by PC-controlled digital-acquisition boards (DAQ) with[85,86] and without[13,42,55,83,89,95] an additional NMR spectrometer. As a minimum, the control software will have to accommodate easy access to the (sometimes overlapping) timings of each step in the polarization procedure, and may extend to acquiring NMR signal *in situ* to facilitate calibrations and improve polarization (*e.g.*, Paravision, LabVIEW,[85–87,92,96] MATLAB[38,95]).

REVIEW OF PUBLISHED INSTRUMENTS

This section comprises a brief description of instrumentation to produce pH$_2$, setups for producing HP solutions, HP of gases, purification methods and translation. The section on setups to produce HP liquids is structured by the magnetic field B_{SOT}, where the SOT takes place.

Parahydrogen generators

As a manifestation of the generalized Pauli exclusion principle, hydrogen molecules exist as two different nuclear spin isomers: the triplet spin states, called orthohydrogen (oH$_2$), and the singlet spin state, called pH$_2$. The energy separation between the ground states of pH$_2$ and oH$_2$ is 170.6 K[83]. Hence, in thermal equilibrium at low temperatures (below 25 K), almost all hydrogen molecules are in the singlet state, *i.e* nearly pure pH$_2$. Note that the temperature determines the achievable pH$_2$-fraction f_{pH2}.

The production of pH$_2$ is straightforward: letting hydrogen gas flow over an ortho-para conversion catalyst at low temperatures results in enriched pH$_2$. Common conversion

catalysts are granular materials with high surface area, such as Fe(OH)O,[28,29,97] nickel sulfate,[98] or chromic oxide (CrO_3) supported on silica gel.[99] Activated charcoal has been used as an ortho-para conversion catalyst in early works, but the efficiency appears to be lower than for the ferromagnetic oxide materials, especially at high flow rates. The catalytic effect originates from (ferro- or para-) magnetic properties, which induce highly inhomogeneous local magnetic fields that accelerate ortho-para conversion.[36]

The published pH_2 generator designs offer different properties with respect to cost, pH_2-fraction, pressure, flow rate and ease of use. Aside from commercial products (Bruker BPHG 90, XeUS Technologies LTD, HyperSpin Scientific UG, Advanced Research Systems, IDB Budzylek), many designs for home-built generators have arisen over the last decades. In particular, three primary coolant technologies dominate: single-stage or dual-stage closed-cycle Helium cryostats operating at 13.5 to 40 K,[29,36,100–104] liquid helium dewars at 14 to 30 K[98,99,105,106] and liquid nitrogen dewars at 77 K.[18,97,107–111] Consequently, a dual stage or liquid-helium-based pH_2 generator can practically reach enrichments approaching 100% and a liquid-nitrogen-based pH_2 generator enrichments of up to 52 %, respectively. In a liquid N_2 generator pumped below ambient pressure, the enrichment can be increased by lowering the temperature further, e.g., to 63 K at 21 mbar allowing a pH_2 fraction of $\approx$ 65 %.[112]

The quantification of the pH_2 enrichment can be done optically (e.g., Raman), or by NMR spectroscopy. Raman spectroscopy is about 500 times faster than NMR and does not require a reference sample since it detects both oH_2 and pH_2 directly.[110] However, NMR spectroscopy is generally the quantification method of choice since it is already available in the MR labs where PHIP experiments are carried out. The details of quantification have been reviewed thoroughly previously.[113]

SOT at tesla fields

SOT conditions. In PASADENA experiments, the hydrogenation reaction, observation, and SOT take place at the high magnetic field of an NMR or MRI system ($\approx$ Tesla). If pH_2 is added at chemically nonequivalent sites, I_1 and I_2 typically become weakly coupled (Figure 2a). The strongly coupled case is typically only present, if $\delta v \approx 0$.[39,114]

For the former case, PHIP ^{1}H signal can be observed as anti-phase peaks by a simple 45° excitation. Alternatively, spin order can be converted into in-phase magnetization using RF pulse sequences[115–117] which also enables detection in inhomogeneous B_0 fields.[118,119] However, the first in-phase PHIP ^{1}H spectra were obtained by Pravica et al. by field cycling (ALTADENA)[49] – an approach that has also enabled polarization transfer to [19]F.[50]

Several techniques have been published to convert $I_{1z}I_{2z}$ into observable magnetization of X-nuclei (often ^{13}C). Here, most RF-SOT sequences are adaptations of the insensitive nuclei enhanced by polarization transfer (INEPT) sequence that considers initial $I_{1z}I_{2z}$ spin order, Figure 2b.[59,120] After the early work from Haake, Natterer and Bargon, who introduced the pH_2 INEPT+ (phINEPT+) sequence,[60] l-PHINEPT+,[51] selective excitation of polarization using PASADENA (SEPP) INEPT,[121] selective-90 (s90) phINEPT[54,122], and efficient SOT to

heteronuclei via relayed INEPT chains (ESOTHERIC, Fig. 2b)[62,82] sequences were suggested. Note that depending on the spin system, and neglecting relaxation, all RF-SOT schemes can yield ~100 % ^{13}C-polarization, in principle, except phINEPT+, which has a theoretical maximum of ~50 % because of the initial 45° [1]H pulse.[38,123] If the initial spin order is $I_1 \cdot I_2$, different SOT schemes are required, e.g. Goldman's sequence[42] for succinate obtained by reacting a fumarate precursor molecule.[39,48] Additional RF-SOT techniques for strongly-coupled protons will be introduced in the next section (SOT at millitesla fields). Adiabatic passages through level anti crossings (also referred to as avoided crossings) were shown to be efficient for the transfer of singlet pH_2 spin order to ^{13}C polarization.[124–126]

Published setups: Various setups for performing PHIP in NMR[94,122] and MRI systems have been described.[38,90] Such implementations offer the advantage that parts of the sophisticated MR machines, including NMR excitation and acquisition and highly homogeneous field over a large volume, can be employed in the hyperpolarization process. Typically, the NMR or MRI system offers TTL outputs that allow control of the fluid path directly from within the pulse program.

To perform the hyperpolarization in an NMR system, Kiryutin et al. introduced a setup consisting of several valves for supplying gases or liquids, e.g., a cleaving agent to convert a precursor into the desired metabolite.[94] Using standard 5 mm or 10 mm NMR tubes for hydrogenation, SOT, detection, and purification, the system can be implemented in all standard and benchtop NMR spectrometers and has been done so by many labs (Figure 2c).[62,119,122,127,128] For in vivo imaging, the HP contrast agent has to be transferred to an imaging system.

Performing hyperpolarization within the bore of an MRI system allows in vivo imaging only seconds after the hydrogenation (SAMBADENA). Here, the hydrogenation takes place in a reactor enclosed in a dual tune, transmit-receive ^{1}H/^{13}C volume coil, equipped with a local receive coil, for RF-SOT and in vivo MRI.[38] The reactor was mounted on the animal bed (with animal warming, vital sign monitoring, anesthesia) such that the contrast agent was delivered directly into a syringe for injection at high field, Figure 2e.[90] In vivo imaging of a sterile solution of hydroxyethyl [1-^{13}C]propionate-d₃ within 15 s after hyperpolarization was demonstrated (Figure 2f), although no purification (i.e. catalyst filtering) was performed.[90]

Published agents: High ^{13}C polarizations for highly concentrated molecules have been demonstrated with phINEPT+ and ESOTHERIC sequences and SAMBADENA.[38,119,127] Promising PHIP agents that were produced at high field with polarization above 10% are tetrafluoropropyl [1-^{13}C]propionate-d₃ (TFPP),[129] [1-^{13}C]succinate-d₂,[39,48] and [2-^{13}C]pyruvate.[130] The latter was achieved using PHIP-SAH, ESOTHERIC and subsequent cleavage of the side arm of cinnamyl [2-^{13}C]pyruvate. Remarkable polarizations were also achieved for other promising PHIP-SAH molecules, namely ethyl [1-^{13}C]acetate[119,127] and cinnamyl [1-^{13}C]pyruvate.[62,82]

Challenges: The main challenges of in situ polarizer setups such as SAMBADENA are due to the limited space within the bore of the MRI or NMR magnet: accommodating production,

5

purification, QA, and the administration within a small volume is not an easy task. RF-SOT sequences - theoretically - achieve ≈ 100 % ^{13}C-polarization, but only in fully ^{2}H-labeled molecules as additional J-couplings will interfere (neglecting relaxation).[38,54,122,127,128] In NMR spectrometers, radiation damping can disturb the SOT, while the limited RF power is a serious concern in MRI setups[119,131–133] because of the large excitation bandwidth needed.[134] Moreover, translational motion of the molecules in the inhomogeneous field of the relatively large reaction chamber in an MRI during SOT can reduce the polarization.[135]
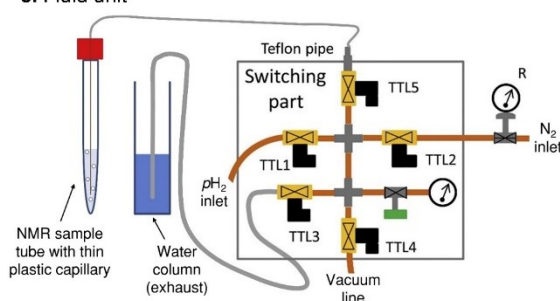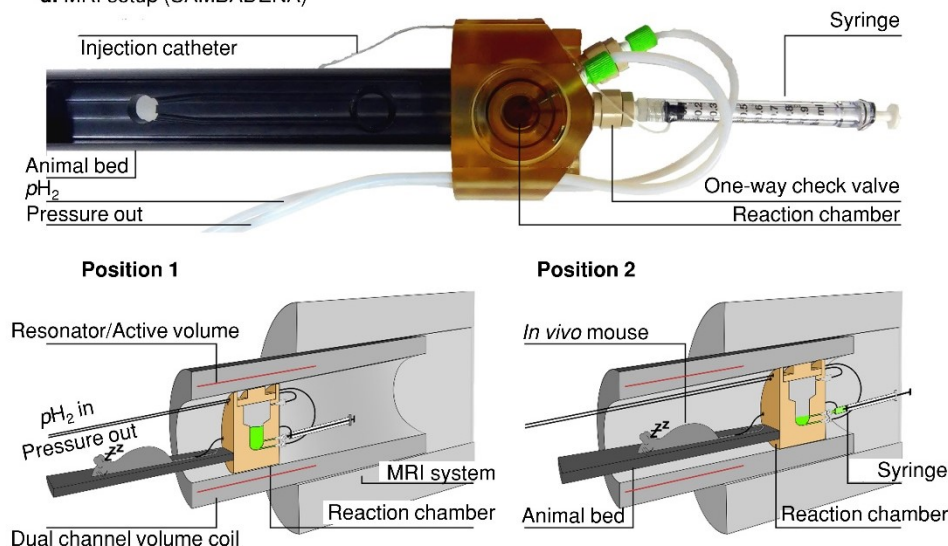

a. Schematic reaction
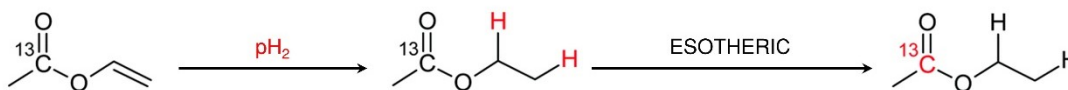
b. High field SOT (ESOTHERIC)
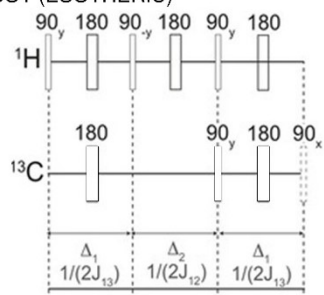
c. Fluid unit

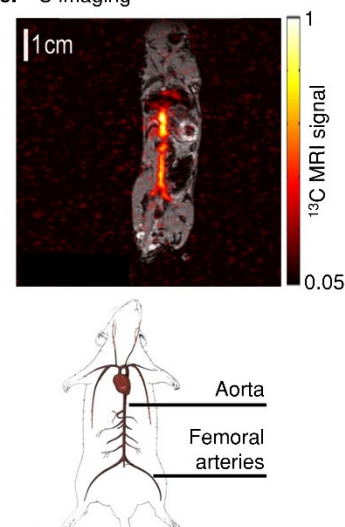**d.** MRI setup (SAMBADENA)

e. ^{13}C imaging

Figure 2. PHIP setups for SOT at constant magnetic fields > 1 T, where spin systems are typically in the weak-coupling regime. Schematic view of the hyperpolarization process at high field, where ethyl acetate is polarized by adding pH₂ (a) and spin order transfer with ESOTHERIC (b) or SLIC. The fluidics are usually handled by a unit consisting of switchable magnetic valves and flow regulation for guiding gases or to apply vacuum to a tube or reactor (c). For MRI systems, dedicated reaction chambers were combined with animal beds allowing animal monitoring, anesthesia, life support and fast administration of the HP contrast agent (d). As an example, sub-second *in vivo* ^{13}C angiography of a mouse was demonstrated only seconds after the polarization (e), while compatible temperature, pressure and sterility was assured. Figure 2a reproduced from Pulsed Magnetic Resonance to Signal-Enhance Metabolites within Seconds by Utilizing Para-Hydrogen, Korchak, S.; Yang, S.; Mamone, S.; Glöggler, S., ChemistryOpen, Vol. 7, Issue 5 (ref 62). Copyright 2018 Wiley. Figure 2b reproduced from Over 50 % 1H and 13C Polarization for Generating Hyperpolarized Metabolites—A Para-Hydrogen Approach, Korchak, S.; Mamone, S.; Glöggler, S. ChemistryOpen, Vol. 7, Issue 9 (ref 127). Copyright 2018 Wiley. Figure 2c reprinted from J. Magn. Reson., Vol. 285 (Supplement C), Kiryutin, A. S.; Sauer, G.; Hadjiali, S.; Yurkovskaya, A. V.; Breitzke, H.; Buntkowsky, G. A Highly Versatile Automatized Setup for Quantitative Measurements of PHIP Enhancements, pp. 26 - 36 (ref 94). Copyright 2017, with permission from Elsevier. Figures 2d and 2e reproduced from In Vivo 13C-MRI Using SAMBADENA, Schmidt, A. B.; Berner, S.; Braig, M.; Zimmermann, M.; Hennig, J.; Elverfeldt, D. von; Hövener, J.-B. PLOS ONE, Vol. 13, Issue 7 (ref 90). Copyright 2018 Public Library of Science.

SOT at millitesla fields

SOT conditions: The characteristic feature of SOT in the millitesla range is the strongly-coupled regime ($\delta v \ll J_{I1I2}$). Typically, the pairwise pH_2 addition takes place under proton decoupling at B_{SOT}, in part to reduce relaxation, but also to preserve the $\mathbf{I_1 \cdot I_2}$ spin order (Figure 3f and Figure 3h). After the decoupling, RF-SOT sequences are used to transfer the spin order to a ^{13}C nucleus. A wide range of efficient pulse sequences have been reported[51,57,58] to accomplish polarization transfer in millitesla field range including the pioneering sequence developed by Goldman and co-workers (Figure 3e).[42,83]

Published setups: As the (^{13}C) hyperpolarization can persist for several minutes, the contrast agent can be transferred from the polarizer to the detector without overwhelming loss, *e.g.*, for polarimetry (*i.e.*, measuring the degree of induced polarization) or ultimate application (*i.e., in vivo* imaging). As a result, several millitesla setups with the main static magnetic field ranging from 1.7 mT[13,89] to 50 mT were set up and reported.[85]

The use of the low magnetic field offers certain advantages: (1) the field can be generated by inexpensive electromagnets, resulting in an overall cost-efficient, portable setup;[92] (2) susceptibility effects are low, and B_0 inhomogeneities can be compensated for by magnet design,[92] shims, and sufficiently strong RF pulses. Utilizing an electromagnet has allowed SOT over large reaction volumes – up to 100 mL were reported[13] – allowing the production of clinical-scale doses of ^{13}C-hyperpolarized contrast agents.[83]

These translational advantages were likely decisive for Amersham Biosciences, a healthcare company, to choose this approach for the first commercial prototype – *in vivo* feasibility studies using the Amersham polarizer have been reported extensively.[42,69,83,136] The overall design of the Amersham polarizer was never reported in detail,[42,83,84,137] but several closely related PHIP millitesla polarizer designs were subsequently reported.[13,36,85–87,89,91–93,96]

As described above, the lifetime of the pH_2-derived ^1H spin order is of the order of seconds and hence, for effective ^{13}C HP, the hydrogenation needs to be completed quickly.[36,138] In practice, fast hydrogenation is achieved through the use of a reactor pressurized to ca. 10 bar with pH_2 followed by a spray injection of a hot stream of precursor solution into the chamber.[13,89] For biomedical applications, the reaction is performed in aqueous media employing water-soluble PHIP catalyst at elevated temperature (70-95 °C).[13,36,86,89,137] As a result, the entire bolus of the precursor molecule can be reacted quickly (in a few seconds), *i.e.*, on a time scale that is faster or similar to the decay of the $\mathbf{I_1 \cdot I_2}$ spin order.

The experimental hardware for the hyperpolarization process is relatively similar among reported millitesla PHIP polarizers (Fig. 1). By definition, such system employs a B_0 magnet operating in the millitesla range with typical field strength of $2 - 9$ mT[13,36,86,89] although the use of higher field (48 mT) permanent magnets have been reported.[85] A large-volume (*ca.* 300 mL) dual-channel RF probe is placed inside the magnet to deliver ^1H and ^{13}C RF pulses for the SOT sequence. The high-pressure reactor is nested inside the dual-channel RF coil – Figure 3c shows an example of such an electromagnet-based polarizer. A millitesla-PHIP polarizer is typically connected to (or contains) cylinders of compressed ultrahigh-purity (>99.999% or 5.0) pH_2 and inert propellant gas (N_2 or Ar). A series of high-pressure valves and tubes form a manifold (Fig. 3a) to fill the reaction chamber with pH_2.[139] This step is followed by the injection of hot precursor solution into the chamber through a nozzle using an inert propellant gas. Various setups were designed to inject a defined amount of the precursor solution into the reaction chamber, and to eject the HP contrast agent into a receiver ready for transfer and *in vivo* MRI. Although specialized heaters were employed to control the reaction temperature, the design shown in Figure 3c employs heating generated by a >100 W electromagnet.

Several approaches were developed to orchestrate the interplay of actuating multiple valves and playing out the RF-SOT, usually including software and a hardware interface (LabVIEW-,[13,36,95,96] Arduino-,[86] Matlab,[95] and NMR spectrometer based[87]). A typical graphical user interface (GUI) allows setting various parameters (reaction time, precursor dose), choosing the SOT sequence, actuating individual valves, and executing various polarization or maintenance routines and sometimes performing NMR (Figure 3b, open-source Arduino-based controller software).[86] All published controller designs have their own merits.

To achieve high and reliable polarization through robust device operation, the accurate and precise application of the RF-SOT is critical.[51] Optimal RF-SOT performance requires calibrated B_1 power and transmission resonance frequencies for both RF channels in particular. Performing these calibrations *in situ* by detecting NMR signal in the reaction chamber using a transmit-receive polarizer design drastically facilitates these procedures. *In situ* calibrations, however, are not necessarily needed to produce the HP agents, because an external (*i.e., ex situ*) NMR spectrometer, MRI scanner or a low-field polarimetry station may be employed for the calibrations,[89] and for probing the achieved ^{13}C polarization level.[69] This so-called transmit-only design is less complex and typically result in a lower device cost as no extra NMR receive hardware is needed. The transmit RF pulses can be generated using simple waveform generators (*e.g.*, NI, Austin, TX, USA), consumer-grade RF amplifiers (WRAT, Onkyo, Osaka, Japan), and untuned RF coils with low Q factor, mitigating radiation damping issues noted in the above section.

The hyperpolarizers employing transmit-receive design were realized by using a commercial, low-frequency, dual-channel NMR spectrometer and dual tune transmit-receive coil (*e.g.*, Kea2, Magritek).[86,87] In another approach, a geometrically decoupled, single or dual tuned receive coil was added to the untuned transmit coil, using the same low-cost waveform generators, amplifiers and ADC/DAC hardware as for the transmit-only design described above.[92,95]

These transmit-receive designs allow using the signal of thermally polarized water to calibrate B_0 and B_1.[86,87,92,95,140] As the polarization of HP samples is independent of the detection field, a high signal-to-noise ratio (SNR) spectrum was readily obtained in in-situ low-field polarimetry as shown for the HP contrast agent [1-^{13}C]phospholactate-d_2 (PLAC) at ~62 kHz (Figure 3d).

While transmit-receive designs are more complex and can be more expensive (by ca. $30,000 for the Kea2), calibration is relatively straightforward, and good reliability and reproducibility of the hyperpolarization yield is achieved.

The efficiency of SOT can be improved further by reducing the complexity of the spin system. For example, deuteration was used to simplify HEP, SUC and PLAC to an effective 3-spin-1/2 system (two nascent protons and one ^{13}C nucleus), which increased the final ^{13}C polarization for PLAC to 15% versus 1% for the fully protonated variant, Figure 3h.[53,141] While deuterium (and phosphorus-31) nuclei possess a spin, they are not excited by the RF and hence not effectively involved in the SOT.[42] In favorable cases, P_{13C} of more than 20 % was achieved with millitesla polarizers,[36,42,137] *e.g.* $P_{13C} = 28\%$ for [1-^{13}C]succinate-d_2 (SUX, Figure 3f,). Despite the enormous signal enhancement provided by hyperpolarization, metabolic imaging with HP contrast agents usually results in low SNR images. Thus, it is not surprising that only deuterated precursors with high P_{13C} were translated to *in vivo* studies using millitesla PHIP polarizers so far.[13,69,83,86,89,142–148]

To date, millitesla-polarizers were employed for *in vivo* ^{13}C MRI or MRS with SUX[147,149] , SUX esters[145], HEP,[5,69,150] and TFPP,[143] and PLAC[86], Figures 3g,i. Thorough reviews covering the *in vivo* applications can be found elsewhere.[113,151]

Two interesting developments, which broaden the scope of polarizable molecules drastically, are PHIP-SAH[20] and PHIP-X.[26] The experimental realizations of these techniques will be described in more detail below, but the millitesla polarizers described here appear to be well positioned for these emerging protocols.

Challenges: The millitesla PHIP polarizers have been shown to be successful devices for the efficient production of HP ^{13}C contrast agents in aqueous media with high P_{13C} exceeding 25% for *in vivo* applications. Using PHIP-SAH molecules may dramatically enlarge the pool of agents, *e.g.*, to ^{13}C-labeled pyruvate. Despite this success, however, all *in vivo* translated precursors so far require deuterated substrates in addition to ^{13}C labeling. While deuteration offers the benefit of a prolonged polarization lifetime, it also increases the cost and the complexity of synthesis of the precursors, which is a clear drawback compared to MFC-SOT. No millitesla polarizer incorporating a purification unit was presented so far.
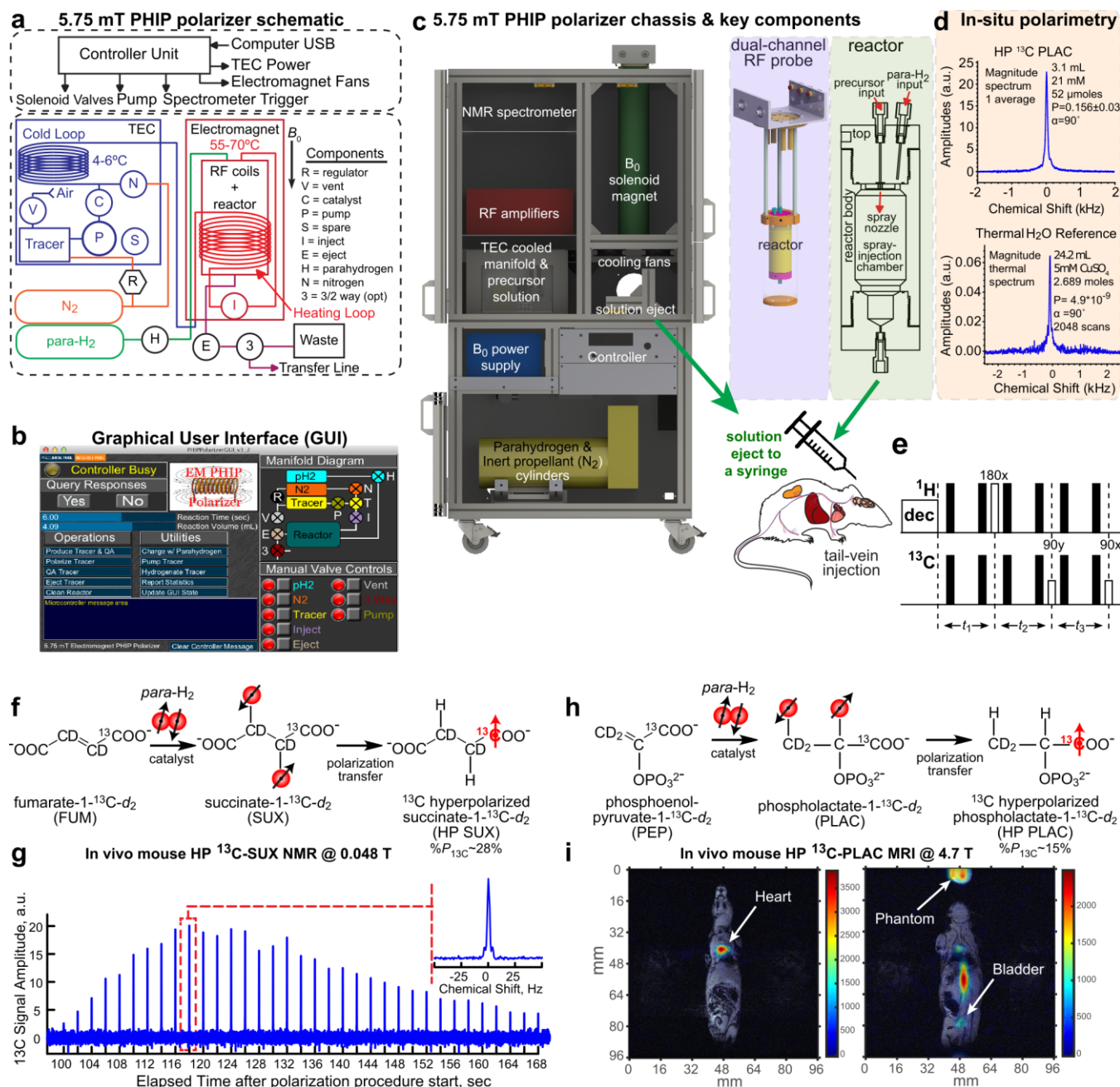
Figure 3. Setups and examples for PHIP at millitesla fields: Overall schematic (a), graphical user interface (b) and rendering (c) of a 5.75 mT automated, pre-clinical, open-source PHIP polarizer. A dual-channel, ^{1}H/^{13}C RF coil was placed inside a B_0 solenoid electromagnet (c, left), and a spray-injection reactor was nested inside the coil. *In situ* NMR detection at ~62 kHz enabled RF calibration and quantification of ^{13}C polarization with respect to thermally polarized water (d). During the hydrogenation reaction of a few seconds, ^{1}H-decoupling was applied to preserve **I·S** spin order, and before the polarization was transferred to ^{13}C using the sequence proposed by Goldman *et al.* (e) – note, that there are only three 'effective' pulses (white) used while the others (gray) are for refocusing of the Zeeman evolution only. Reaction scheme (f) and *in vivo* ^{13}C-NMR (g) of contrast agent SUX detected at low magnetic fields (~0.048 T). Reaction scheme (h) and *in vivo* ^{13}C MRI imaging (i) of contrast agent PLAC at 4.7 T: ^{13}C-MRI (color) was acquired approximately 5 − 10 s after the injection of ~0.2 mL, ~30 mM hyperpolarized PLAC into the tail vein of a healthy nude mouse (prior tumor implantation) and overlaid on representative ^{1}H images (gray scale, ^{13}C: GRE, 3 x 3 mm^2 in-plane resolution, 6 mm slice thickness, FOV = 96 x 96 mm^2). Figures 3a-d, 3h and 3i reproduced from Coffey, A. M.; Shchepin, R. V.; Truong, M. L.; Wilkens, K.; Pham, W.; Chekmenev, E. Y. Open-Source Automated Parahydrogen Hyperpolarizer for Molecular Imaging Using 13C Metabolic Contrast Agents. Anal. Chem. 2016, 88, 8279–8288 (ref. 86). Copyright 2016 American Chemical Society. Copyright 2006, with permission from Elsevier. Figures 3f and 3g reprinted from J. Magn. Reson., Vol. 281 (Supplement C), Coffey, A. M.; Feldman, M. A.; Shchepin, R. V.; Barskiy, D. A.; Truong, M. L.; Pham, W.; Chekmenev, E. Y. High-

9

Resolution Hyperpolarized in Vivo Metabolic 13C Spectroscopy at Low Magnetic Field (48.7mT) Following Murine Tail-Vein Injection, pp. 246 - 252 (ref 147). Copyright 2017, with permission from Elsevier.

SOT at ultralow fields (ULF)

SOT conditions: At ultra-low fields (micro- or nanotesla), the frequency differences between heteronuclei and protons (γ_{1H}-γ_X) are reduced to be in the order of the *J*-couplings or below. At such low fields, a spin bath between all spin-spin coupled nuclei is effectively established through which polarization can easily propagate spontaneously. In other words, if a part of a nuclear spin network is initialized in the singlet state via pH$_2$, and the Zeeman interactions are negligible compared to the *J*-couplings, then the polarization spreads through the network.[152,153] The beauty of this "spontaneous" polarization transfer approach is that it is general and does not require specialized pulse sequences that are highly dependent on the specific spin system under study. Note that this concept was realized early on, when the so-called ALTADENA approach was established,[49] where pH$_2$ was introduced into the spin system through hydrogenation and polarization "flows" to other ^{1}H spins at millitesla fields or below,[154] as mentioned in the section above and is theoretically analysed in the following section. However, to polarize a spin-1/2 heteronucleus, such as ^{13}C, ^{15}N, ^{31}P, *etc.*, ultra-low microtesla fields are required to strongly couple the protons of the spin system with the target X-nucleus to allow spontaneous polarization transfer. Over the last decade, a wide variety of experiments have been demonstrated taking advantage of this heteronuclear spin bath at microtesla fields, including hydrogenative[20,124,155–160] and non-hydrogenative PHIP.[161–164] Newest approaches have used pulse sequences at microtesla fields,[125,165–167] which can focus polarization transfer in a more targeted way to specific nuclei, but become highly dependent on the specific spin system under study.

Published setups: While dedicated setups to produce diagnostically relevant contrast agent have not yet emerged, some interesting setups were described that allow exploiting the unique properties at these fields. Among these are (a) the distribution of the polarization across an entire molecule and different coherences,[106] (b), the unique sensors to detect signals in the Hz – kHz range, [168–170] and (c) the identification of molecules by their *J*-couplings rather than their chemical shift.[171–173]

To establish magnetic fields below the Earth's field, entering nanotesla to microtesla field regimes, typically mu-metal shields are used.[168,174] Inside such shielding, well-defined magnetic fields are commonly generated with conventional resistive coils in Helmholtz, solenoid or other configurations driven by low noise current sources.

To acquire HP spectra (typically from small molecules in solution), a variety of ULF MR setups have been designed, Figure 4. The detection sensitivity for conventional RF coils, as used for high field MR experiments, decreases with frequency.[175] Therefore, at ultralow fields different magnetic field detectors such as atomic magnetometers (Figure 4a),[152,153,169,174,176,177] or superconducting quantum interference devices (SQUIDs) (Figure 4b)[168,178] may be more sensitive than inductive detection. Such sensors are even sensitive enough to perform magnetoencephalography,[179] but can also be used to detect nuclear spins. They can operate as broad band detectors (SQUIDs: DC – ≈1 GHz, atomic magnetometers: DC – ≈1 kHz), where no matching and tuning is required and the MR signal of different nuclei such as ^{13}C, ^{15}N, ^{19}F and ^{1}H can be detected simultaneously.[106]

More recently, fluorescent nitrogen vacancy (NV) centers in diamonds (Figure 4c) have also been used to detect PHIP signal. While the NV centers typically have less absolute magnetic field sensitivity, the advantage is that they can be brought in direct contact with the solution (unlike SQUIDS or atomic magnetometers).[170,180] These can also be used for magnetometry at zero field.[181]

The linewidth of the detected MR signals for ULF setups can be less than 1 Hz down to tens of mHz,[171] so that *J*-couplings can be easily resolved. Narrow linewidths are obtained since field inhomogeneities decrease with the field strength, which enables chemically specific, high resolution J-coupling spectroscopy.

Challenges: Generating and detecting HP signals at ULF offers unique insights into the investigated spin systems and provides NMR and MRI without requiring superconducting magnets. However, a disadvantage of all ULF detection methods remains, which is the frequency-dependent noise of the sensors (SQUIDs ≈ 1 fT/Hz$^{-1/2}$, atomic magnetometers ≈ 10 fT/Hz$^{-1/2}$). Accordingly, there is an ongoing quest to decrease the noise level below the sample noise. Moreover, medically viable polarizers or sensors that take advantage of PHIP at ULF have not emerged yet. The aspiration remains that the described discoveries and techniques will soon be translated into broad application.
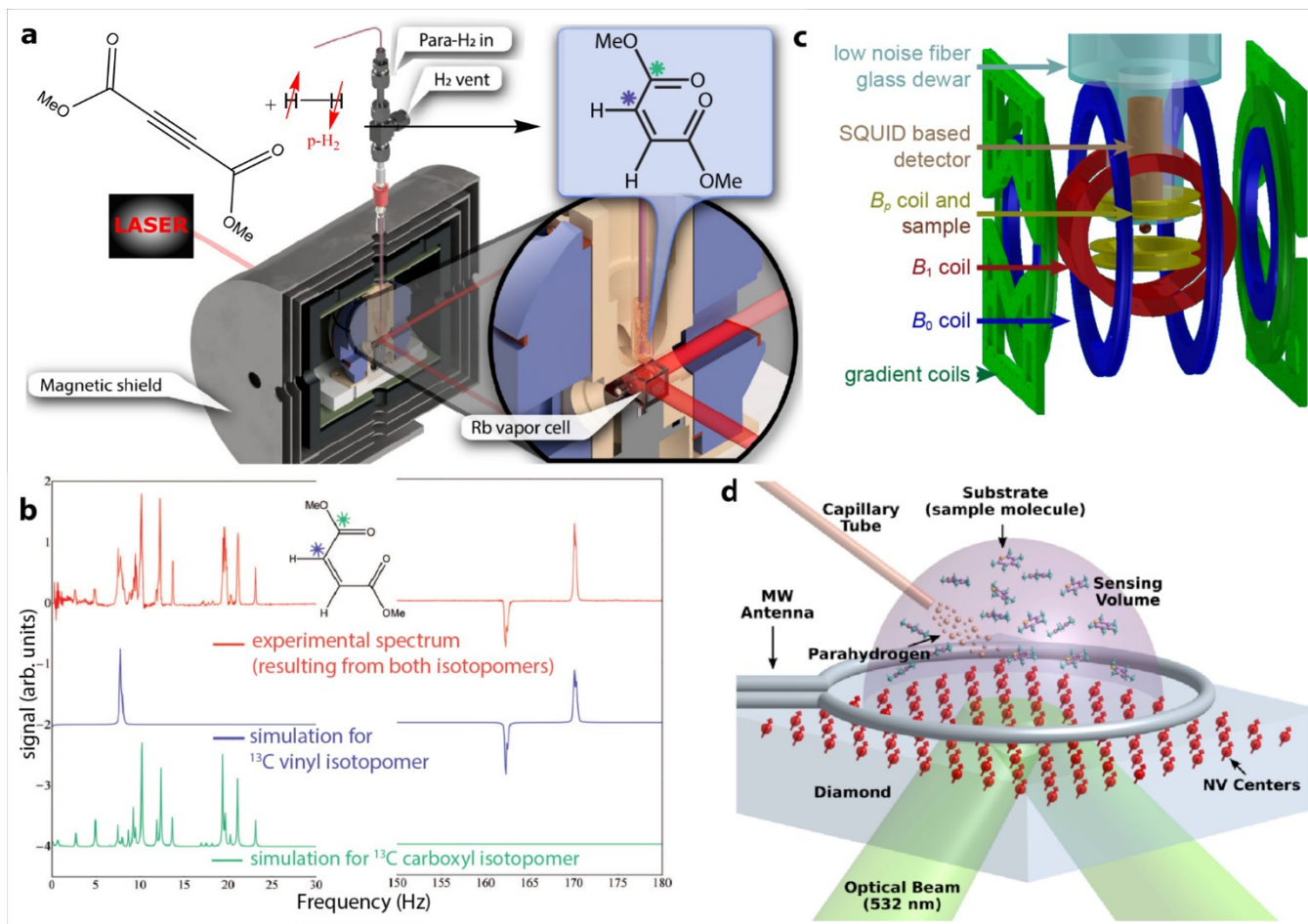
Figure 4. Setups and examples suitable for PHIP at ULF. (a) atomic magnetometer system based on a Rb vapor cell. (b) PHIP enhanced zero field NMR spectrum of dimethyl maleate acquired with a Rb vapor magnetometer. (c) SQUID based system. (d) optically probed nitrogen-vacancy (NV)-NMR spectrometer. Figure 4a reproduced from Towards Large-Scale Steady-State Enhanced Nuclear Magnetization with in Situ Detection, Blanchard, J. W.; Ripka, B.; Suslick, B. A.; Gelevski, D.; Wu, T.; Münnemann, K.; Barskiy, D. A.; Budker, D.Magn. Reson. Chem., Vol. -, Issue - (ref 169). Copyright 2021 Wiley. Figure 4b reprinted from Parahydrogen-Induced Polarization at Zero Magnetic Field, Butler, M. C.; Kervern, G.; Theis, T.; Ledbetter, M. P.; Ganssle, P. J.; Blanchard, J. W.; Budker, D.; Pines, A., J. Chem. Phys., 2013, Vol. 138, Issue 23 (ref 152), with permission of AIP Publishing. Figure 4c reprinted from Mutual Benefit Achieved by Combining Ultralow-Field Magnetic Resonance and Hyperpolarizing Techniques,Buckenmaier, K.; Rudolph, M.; Fehling, P.; Steffen, T.; Back, C.; Bernard, R.; Pohmann, R.; Bernarding, J.; Kleiner, R.; Koelle, D.; Plaumann, M.; Scheffler, K., J. Rev. Sci. Instrum., 2018, Vol. 89, Issue 12 (ref 168), with permission of AIP Publishing. Figure 4d reproduced from Micron-Scale NV-NMR Spectroscopy with Signal Amplification by Reversible Exchange, Arunkumar, N.; Bucher, D. B.; Turner, M. J.; TomHon, P.; Glenn, D.; Lehmkuhl, S.; Lukin, M. D.; Park, H.; Rosen, M. S.; Theis, T.; Walsworth, R. L., PRX Quantum, Vol. 2, Issue 1 (ref 170). Copyright 2021 American Physical Society.

Magnetic field cycling (MFC)

SOT conditions: MFC is another method that is widely used for the polarization transfer from $I_1 \cdot I_2$ spin order to heteronuclei. In contrast to the previous sections, which dealt with SOT at a constant magnetic field B_0, MFC exploits varying the magnetic field from values close to geomagnetic field (30-50 µT) to nearly zero field, and a few T. MFC-SOT was the first method to produce net ^{1}H magnetization[49] and used to produce the first ^{13}C *in vivo* MRI in 2001.[5] The method is not to be confused with the fast field cycling relaxometry where the magnetic field is varied to investigate relaxation or spin-state evolution at a low magnetic field in order to gain information about physical or chemical properties of the system under study.[182] For PHIP, a MFC process does not explicitly require *in situ* signal detection, although some setups do this.[88]

To give an idea of the effect of MFC on the spin state populations in PHIP-polarized molecules, we consider a three-spin system formed by two pH$_2$ protons (H and H') and a heteronucleus (X). The spin states can be conveniently described using the singlet-triplet-Zeeman basis. The eight basis states are:

$$|T_+\alpha\rangle = |\alpha\alpha\alpha\rangle, |T_+\beta\rangle = |\alpha\alpha\beta\rangle,$$

$$|T_0\alpha\rangle = \frac{1}{\sqrt{2}}|(\alpha\beta + \beta\alpha)\alpha\rangle, |T_0\beta\rangle = \frac{1}{\sqrt{2}}|(\alpha\beta + \beta\alpha)\beta\rangle,$$

$$|S_0\alpha\rangle = \tfrac{1}{\sqrt{2}}|(\alpha\beta - \beta\alpha)\alpha\rangle, |S_0\beta\rangle = \tfrac{1}{\sqrt{2}}|(\alpha\beta - \beta\alpha)\beta\rangle,$$

$$|T_-\alpha\rangle = |\beta\beta\alpha\rangle, |T_-\beta\rangle = |\beta\beta\beta\rangle,$$

where the first letter refers to the proton spin state, and the second refers to the heteronuclear spin state.

Upon pH_2 addition to a precursor at geomagnetic fields the states $|S_0\alpha\rangle$ and $|S_0\beta\rangle$ are populated almost equally. At these "higher" fields, the ^1H and heteronuclei are weakly coupled and no heteronuclear magnetization is obtained, because to a good approximation only the $|T_0\alpha\rangle$-$|S_0\alpha\rangle$ states and the $|T_0\beta\rangle$-$|S_0\beta\rangle$ states are mixed. However, when the magnetic field is low enough such that the difference in proton and heteronuclear Larmor frequencies approximately matches the J-coupling frequencies, the states with equal angular momentum projection along the field axis (z): $|T_+\beta\rangle$, $|T_0\alpha\rangle$, $|S_0\alpha\rangle$, and $|T_-\alpha\rangle$, $|T_0\beta\rangle$, $|S_0\beta\rangle$ are mixed. This leads to level anticrossings (LACs) between the relevant states, and by varying the magnetic field either rapidly (diabatic passage) or slowly (adiabatic passage), it is possible to transfer spin state populations between the eigenstates.[183] The spin state energies and populations are shown in Figure 5a, and the relevant Hamiltonians are reported in ref. [156].

In the most common example of MFC, the hydrogenation reaction using pH_2 is carried out in the laboratory field (usually tens of microtesla), which is high enough to prevent leakage of proton spin order onto heteronuclear spins, but low enough that proton chemical shift differences, which would lead to loss of spin order, are suppressed, *i.e.*, the protons remain strongly coupled. The field is then diabatically (rapidly) reduced to near-zero field, and then adiabatically (slowly) increased to the tesla range, such that the spin state populations follow the eigenstates as the field passes through the LACs. Overall, this process leads to $I_1 \cdot I_2$ order being transformed into both proton and heteronuclear magnetization. For biomedical applications, it is the heteronuclear Zeeman order that is of interest, although we note that the protons are also polarized by this process, Figure 5a.

Published setups: The most basic MFC experiment is a hydrogenation in a few millitesla followed by transfer to a few tesla for detection.[49] To transfer polarization to X-nuclei, a mu-metal chamber can be used to reach near-zero field conditions (nanotesla). The two passages can be achieved manually, by dropping the sample after hydrogenation into the shield (diabatic passage) and lifting it out slowly (adiabatic passage).[5] In more sophisticated setups, the speed of passages is controlled by means of an electromagnet inside the mu-metal shield.[157,184] The use of coils allows more-precise control over the magnetic fields and has become a routine approach for MFC. A schematic of an experimental apparatus used for MFC is shown in Figure 5b.

The approach was first introduced experimentally by K. Golman *et al.* in 2001.[5,55] After pairwise addition of pH_2, the sample was (rapidly) dropped into a three-layer mu-metal shield at < 100 nT and then slowly lifted at approximately 10 cm/s rate. Using this method, the authors generated 4 % ^{13}C polarization on [1-^{13}C]maleic acid dimethyl ester. A more thorough theoretical explanation of the technique and description of the setup followed,[55,137] now including coils inside the magnetic shield to provide time-dependent variable fields. The magnetic field was initially held at 100 μT as the

hydrogenated sample was inserted into the shield, then diabatically reduced to 30 nT in about 1 ms, and then exponentially ramped back to 100 μT on the order of seconds. This approach, in combination with a spray-injection chamber for the hydrogenation with pH_2, led to ^{13}C polarization on hydroxyethyl-propionate of ≈21 %. In later work, this experimental apparatus was used to produce HP ^{13}C contrast agents for coronary angiography imaging in pigs.[150]

There is merit to the approach of shuttling samples in and out of a magnetic shield by hand in the simplicity and low experimental requirements, and this approach was employed to hyperpolarize different heteronuclei such as ^{13}C,[185] ^{15}N,[186] and ^{129}Si.[187] A few years later, this approach was employed to hyperpolarize the ^{13}C spins in a number of molecules, including pyruvate and acetate, by means of PHIP-SAH.[20,56] A detailed description of a coil-based magnetic field cycling setup was provided by Shchepin *et al.* where they studied the dependence of ^{13}C polarization in [1-^{13}C]ethyl acetate on the minimum field used during the MFC.[184] They demonstrated that the MFC should reach fields below 1 μT for efficient ^{13}C polarization. Using this optimized coil-based approach, the ^{13}C polarization of [1-^{13}C]pyruvate generated via side-arm hydrogenation was improved from 2.3 %[20,56] to 8.3 %,[157] and the method was also applied for hyperpolarizing [1-^{13}C]fumarate (FUM).[24,188]

In FUM, derived from hydrogenation of ADC (acetylene dicarboxylic acid), an AA'X spin system is formed.[189] Because of its simplicity, the system is useful for studying and optimizing MFC methods. It was on this molecular system that a MFC variant known as magnetic field sweeping was tested.[156] In this method, rather than a diabatic field reduction followed by an adiabatic increase, the magnetic field is inverted adiabatically, *i.e.*, passing through zero field. The field sweeping method was then applied to hyperpolarize vinyl-acetate, and the effect of the magnetic field sweep step size and rate was investigated.[88] The authors found that for MFCs using a field range of a few microtesla, a sweep rate of 50 steps/μT/s was sufficient, with higher values leading to no improvement. Magnetic field sweeping does not need rapid field changes, and hence seems more amenable for application to liquids under continuous flow. Its lower efficiency with respect to field cycling,[156] is likely due to the deleterious effects of transverse magnetic fields when passing through the zero-field point, and hence in future work an MFC approach was used for generating HP FUM.[24,188]

This molecular system was also used to study the benefits of constant-adiabaticity methods for MFC and field sweeping.[190] Under the constant-adiabaticity constraint, the magnetic field variations are slow at the LAC field, but the field can be varied more rapidly away from this key feature. This is particularly useful for spin systems that relax rapidly during the MFC process.

Challenges: More complicated molecular systems can present some pitfall to the application of MFC, in particular when quadrupolar nuclei such as ^2H[191] or ^{14}N[186] are J-coupled to the pH_2–derived protons. The strong-coupling condition that is reached at nearly zero field brings these heteronuclei in contact with the spin order of pH_2 and quadrupolar relaxation can work as a hyperpolarization sink.

Another caveat to be considered is that exposure to magnetic fields magnetizes the mu-metal, and so the magnetic shielding should be periodically degaussed to ensure the near-zero field condition is met inside it. In cases where the magnetic shield is near a high-field magnet, it is common to use active shimming with coils inside the shield to achieve the near-zero field condition.
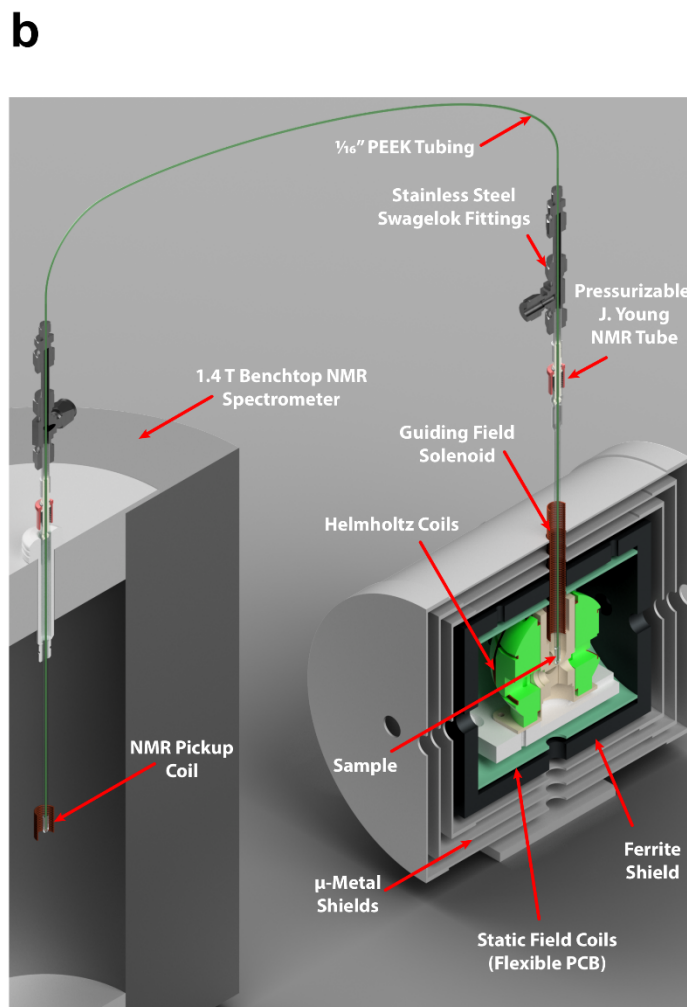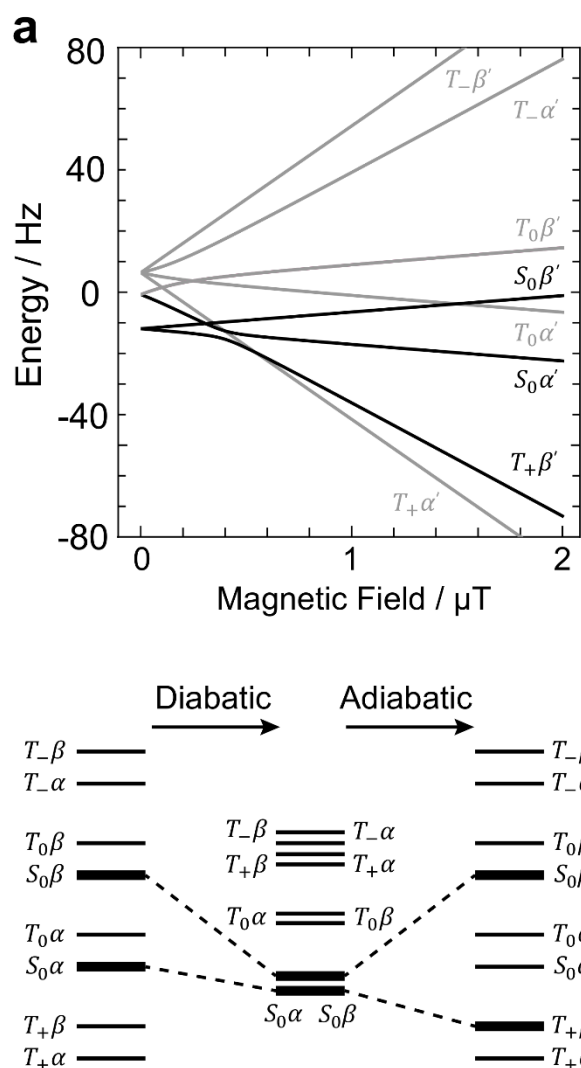

Figure 5. Diagrams and Setups for PHIP by MFC. (a) Energies of the eigenstates of [1-^{13}C]fumarate, plotted as a function of magnetic field strength, with states relevant to MFC-SOT highlighted in black (top). In an ideal MFC, the pH$_2$-derived singlet order $\mathbf{I_1 \cdot I_2}$ is converted into heteronuclear magnetization by first diabatic passage to near-zero-field, followed by adiabatic passage back to microtesla field (bottom). The diabatic passage preserves the state of the system with the protons in a singlet state (*i.e.*, $|S_0\alpha\rangle$ and $|S_0\beta\rangle$), but during the subsequent adiabatic return to high field the state $|S_0\alpha\rangle$ evolves into $|T_+\beta\rangle$, meaning some degree of proton singlet order is lost, but heteronuclear polarization in the β state is gained. (b) Illustration of a polarizer where a sample is polarized by MFC or field sweeping and transferred to an NMR system for detection. Figure reprinted from Polarization Transfer via Field Sweeping in Parahydrogen-Enhanced Nuclear Magnetic Resonance, Eills, J.; Blanchard, J. W.; Wu, T.; Bengs, C.; Hollenbach, J.; Budker, D.; Levitt, M. H., J. Chem. Phys., 2019, Vol. 150, Issue 17 (ref 156), with permission of AIP Publishing.

PHIP OF GASES

While low sensitivity of NMR often is an issue, it is particularly severe for gases as their densities at ambient pressure are *ca.* 1000-fold lower compared to liquids. PHIP has been applied to produce HP molecules in the gas phase[15,16,192] - mostly gases, but also vapors of volatile liquids and even solids.

One approach is to use a solution of a metal complex in a homogeneous hydrogenation with subsequent transfer of the target species to gas phase. For instance, aqueous stoichiometric hydrogenation of norbornadiene resulted in the release of water-insoluble hyperpolarized norbornene to the gas phase.[193] Bubbling of a mixture of pH$_2$ with propylene (propyne, *etc.*) through a solution of a rhodium or iridium complex was used to

produce polarized gases.[194] Another approach relies on the use of solid catalysts to produce PHIP in heterogeneous hydrogenations (HET-PHIP). By bubbling pH$_2$ through a suitable volatile liquid, pH$_2$ is saturated with its vapor, and this gaseous mixture is then supplied to a cell with a solid catalyst for hydrogenation. Often, unsaturated gases premixed with pH$_2$ are used in HET-PHIP experiments.

Published setups: Published examples include hydrogenation of vinyl acetate vapors over a Rh/TiO$_2$ catalyst with subsequent dissolution and hydrolysis of ethyl acetate to hyperpolarized ethanol and acetate,[195] and hydrogenation of vinylethyl ether to hyperpolarized diethyl ether, a known inhalable anesthetic.[196] Unsaturated gases are simply premixed with pH$_2$ and supplied to a catalytic reactor to yield a continuous stream of hyperpolarized gas.[15,16,192,197]

The experiments with gases can be performed under PASADENA or ALTADENA condition. For propane (H$_3$C-CH$_2$-CH$_3$) produced upon hydrogenation of propylene (H$_2$C=CH-CH$_3$), in PASADENA experiments, a pair of enhanced antiphase multiplets is observed with an admixture of in-phase contributions of opposite sign for the two signals. In ALTADENA experiments with hydrogenation at the Earth's field, where all ^{1}H spins in a product molecule are strongly coupled, transfer of the gas to the NMR probe results in the observation of polarization for all coupled ^{1}H nuclei. For propyne hydrogenation to propylene, it is possible to estimate the stereoselectivity of the hydrogenation by fitting the experimental spectra to ALTADENA numerical simulations, which would be otherwise impossible for this reaction.[198] The adiabatic condition of low-to-high field transfer is seldom met fully with gases as T_1 times are short, and slow transfer leads to major polarization losses. Short relaxation times in the gas phase are due to spin-rotation interaction, which also makes the T_1 of heteronuclei shorter than for protons. As a result, polarization transfer from ^{1}H to heteronuclei is impractical even though its feasibility has been demonstrated.[199]

PASADENA experiments with gases are particularly easy to implement – the substrate gas and pH$_2$ (and, if required, a diluent gas, *e.g.*, N$_2$) can be premixed in a gas cylinder or supplied by combining the outputs of mass flow controllers, and the hydrogenation reaction performed in an NMR tube containing a solid catalyst, its suspension in a liquid, or a solution of a suitable transition metal complex. ALTADENA experiments provide a much broader flexibility in experimental conditions, Figure 6a. A reactor can be as simple as a temperature-controlled section of stainless steel or copper tubing or a quartz U-tube containing solid catalyst powder which is held in place by glass wool plugs. It is important to monitor the reactor bed temperature as hydrogenation is exothermic and run-away heating effects are possible. The gas is supplied via gas lines from a gas cylinder to the reactor and then from the reactor to the NMR tube and eventually towards the exhaust; all connections should be gas-tight to avoid gas leaks, and all components should withstand the required gas pressures. Commercially available flow NMR probes, popularized with the advent of liquid chromatography (LC) NMR, are well suited for acquiring the spectra on aliquots of the flowing hyperpolarized gases. However, gas flow rates through the smaller coil volumes of these probes need to be reduced accordingly to avoid residence-time line-broadening. Such effects can also be averted with an interrupted-flow system where the gas flow is allowed to bypass the probe during NMR acquisition while not perturbing the steady-state of the reactor bed. This is also a useful way to isolate a gas sample in the probe to acquire thermally equilibrated spectra. A provision for heating the reactor and catalyst pretreatment in a stream of H$_2$ or gas mixtures is useful. A somewhat more sophisticated setup was designed[200] for a controlled clinical-scale (>300 mL in 2 s) batch production of HP propane (Figure 6c), which makes provisions for efficient preheating of reactants and subsequent dissipation of heat produced in the highly exothermic hydrogenation reaction, as well as for operation at elevated pressures (~ 8 bar).

HP norbornene vapor was produced from an aqueous solution of Rh(I) complex incorporating a norbornadiene ligand by either bubbling pH$_2$ through it (for high-field NMR; Figure 6d) or by spraying it into a chamber pressurized with pH$_2$ (for NMR at 47.5 mT; Figure 6e).[193] Gas-liquid biphasic hydrogenations employed a dissolved catalyst, and gaseous reactants were bubbled through the solution, Figure 6b. The reaction product returned to the gas phase and retained a significant level of hyperpolarization, providing a complete separation of the hyperpolarized substance from the catalyst.[194]

Prepolarized propane was used in many studies to image voids in various objects[201–203] including microfluidic devices.[204,205] Imaging of HP reaction products formed in an operating model catalytic reactor facilitates mapping of their spatial distribution within the catalyst bed.[206–209]

Challenges: The main challenge with gases is the short T_1 time; for propane it is below 1 s at 9.4 T and 1 bar, but depends strongly on pressure and gas mixture composition.[210] T_1 times tend to be longer for shorter molecular rotational correlation times, *i.e.*, for larger and/or heavier molecules, higher gas pressures, or gases in small pores. The T_1 values of small gas molecules generally increase upon dissolution in liquids. For example, $T_1 \approx 1$ ms for H$_2$ gas at 1 bar but it increases by ca. 1000-fold upon dissolution in methanol-d$_4$. Condensation of hyperpolarized diethyl ether vapor was also shown to prolong hyperpolarization lifetime.[196] Furthermore, because of the strong coupling for protons at low fields, they can exhibit properties of long-lived spin states (LLSS).[211] For instance, measurements at 0.05 T for propane gas gave $T_{LLSS}/T_1 \approx 3.1$ at 3 - 7.6 bar, with $T_1 \approx 4$ s and $T_{LLSS} \approx 13$ s at 7.6 bar.[212] Similar trends were reported for diethyl ether vapor.[213] The spin-lock induced crossing (SLIC) pulse sequence can be conveniently used to convert LLSS to an observable signal.[212,213] Another challenge with heterogeneous hydrogenation is that it is outperformed by its homogeneous counterpart in the polarization levels achieved due to low selectivity to pairwise H$_2$ addition, often $P_{1H} = 1 – 3$ % or even lower. Values of $P_{1H} = 7 – 10$ %[203,214–216] or even 60 %[217] have been reported using heterogeneous catalysis, but in most cases accompanied by low levels of catalytic conversion.
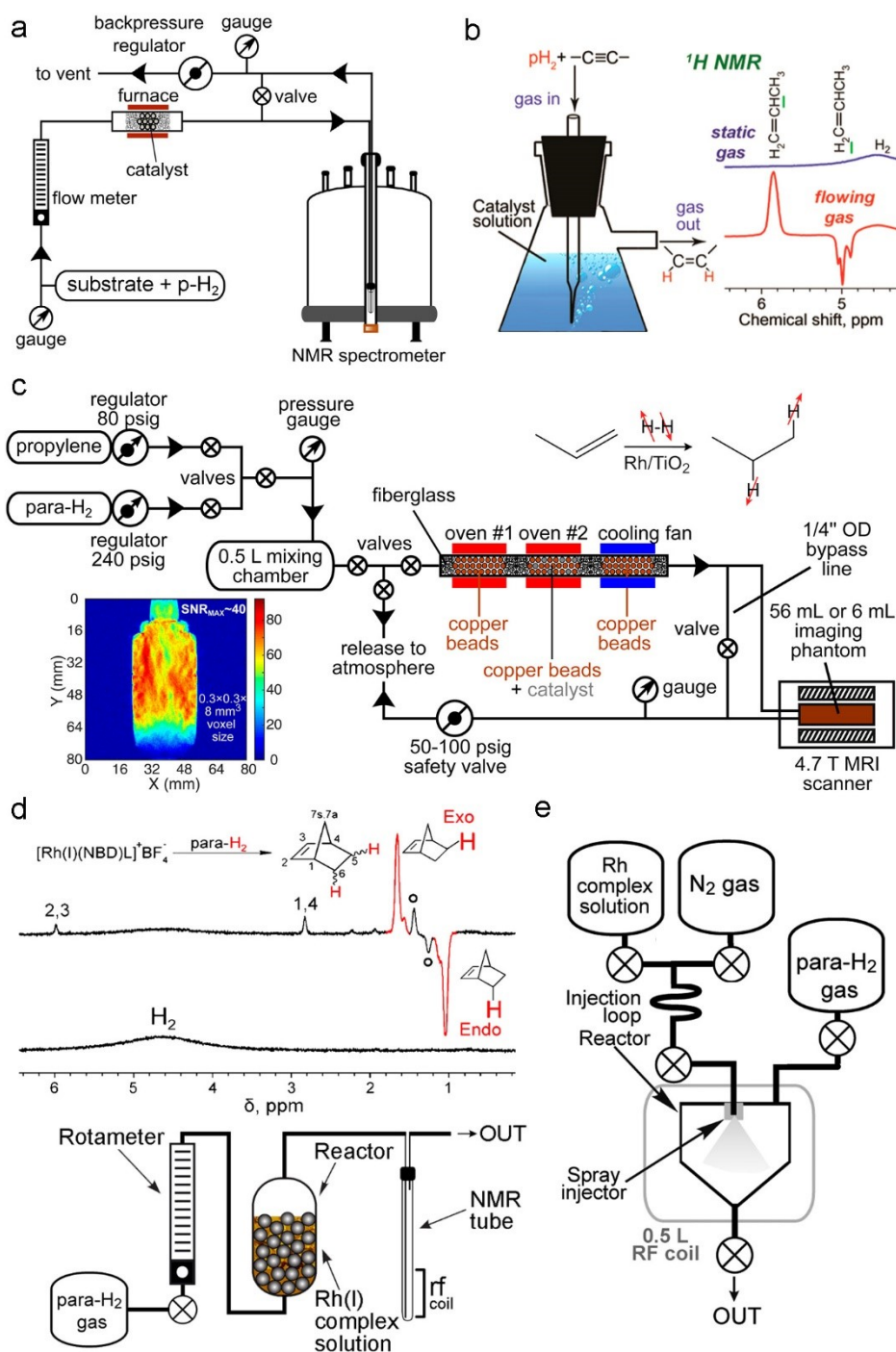
Figure 6. Setups for PHIP of gases. a) Experimental setup employed for producing hyperpolarized gases or vapors via heterogeneous hydrogenation of unsaturated precursors premixed with pH$_2$. b) Schematics of an experimental setup (left) for biphasic hydrogenation of gases upon bubbling their mixture with pH$_2$ through a homogeneous solution of metal complex catalyst, with the hyperpolarized product continuously escaping into the gas phase. The spectra shown as an example (right) are for biphasic hydrogenation of propyne to propylene. c) Schematics of a more advanced experimental setup used for a rapid batch-mode production and MRI detection of hyperpolarized propane gas. The insets show the reaction scheme (top-right) and a gradient echo 2D MR image of ~200 mL of hyperpolarized propane gas in an ~56 mL container acquired at 4.7 T (bottom-left). d) The diagram of the experimental setup used to produce hyperpolarized vapor of norbornene by bubbling pH$_2$ through an aqueous solution of a Rh(I) complex possessing a norbornadiene ligand (bottom), the reaction scheme (top), and the resulting gas-phase ^{1}H NMR spectra (middle). Open circles label the signals of norbornane. Plastic spheres in the reactor were used to reduce its volume. e) The diagram of the experimental setup used for injecting Rh(I) complex solution into a 56-mL volume containing pH$_2$ at ≈7 bar pressure for subsequent *in situ* ^{1}H NMR spectroscopy of hyperpolarized norbornene at 47.5 mT. Figure 6a reproduced from Heterogeneous Parahydrogen-Induced Polarization of Diethyl Ether for Magnetic Resonance Imaging Applications, Salnikov, O. G.; Svyatova, A.; Kovtunova, L. M.; Chukanov, N. V.; Bukhtiyarov, V. I.; Kovtunov, K. V.; Chekmenev, E. Y.; Koptyug, I. V. Angew. Chem. Int. Ed. Engl., Vol. 27, Issue 4 (ref 196).

Copyright 2021 Wiley. Figure 6b reproduced from Kovtunov, K. V.; Zhivonitko, V. V.; Skovpin, I. V.; Barskiy, D. A.; Salnikov, O. G.; Koptyug, I. V. Toward Continuous Production of Catalyst-Free Hyperpolarized Fluids Based on Biphasic and Heterogeneous Hydrogenations with Parahydrogen. J. Phys. Chem. C 2013, 117 (44), 22887–22893 (ref. 194). Copyright 2013 American Chemical Society. Figure 6c reproduced from Salnikov, O. G.; Nikolaou, P.; Ariyasingha, N. M.; Kovtunov, K. V.; Koptyug, I. V.; Chekmenev, E. Y. Clinical-Scale Batch-Mode Production of Hyperpolarized Propane Gas for MRI. Anal. Chem. 2019, 91 (7), 4741–4746 (ref. 200). Copyright 2019 American Chemical Society. Figures 6d and 6e reproduced from Kovtunov, K. V.; Barskiy, D. A.; Shchepin, R. V.; Coffey, A. M.; Waddell, K. W.; Koptyug, I. V.; Chekmenev, E. Y. Demonstration of Heterogeneous Parahydrogen Induced Polarization Using Hyperpolarized Agent Migration from Dissolved Rh(I) Complex to Gas Phase. Anal. Chem. 2014, 86 (13), 6192–6196 (ref. 193). Copyright 2014 American Chemical Society.

PURIFICATION

As soon as the development of PHIP as a hyperpolarization method for metabolic MRI began,[5,137] it became apparent that purification of the reaction solution would be necessary for preclinical and clinical *in vivo* applications. In this regard, PHIP presents some challenges. As outlined above, the hyperpolarization often requires rather non-physiological conditions (organic solvents, pH value, temperature) and high concentrations of organometallic catalysts.[5,13,14,20,24,89,127,128,137,149] Moreover, the hydrogenation reaction may be incomplete or lead to side products.[24] Hence, purifying the polarized solution is important and - keeping in mind the short lifetime of liquid-state hyperpolarization - needs to be performed as quickly as possible, ideally within a few tens of seconds. Many purification strategies exist in chemistry already and some were adapted to PHIP as described below.

Catalyst scavenging

One way to remove the catalyst is metal scavenging. In this approach, the scavenger is either used in a filtration column or mixed with the reaction solution and subsequently filtered out.[81,114,137,218] A commercially available metal scavenger (QuadraPure TU) was employed to clean a solution of HP fumarate prior to *in vivo* MRI.[114] Near complete removal of ruthenium was achieved by slowly passing the solution through the scavenger in about a minute, but a reduction of concentration from ~7 g/L to 100 mg/L was reached within seconds.[114] Similar scavenging approaches have been introduced by Kidd *et al.*[218] and Barskiy *et al.*[81] to remove an iridium-based SABRE catalyst.

A shortcoming of metal scavenging is that although the catalyst is removed, unreacted starting materials and side products may remain. Nevertheless, it was found to be a useful step for reducing the remaining metal contamination further in already purified solutions.[81]

Liquid-liquid phase separation:

Liquid-liquid (LL) phase extraction was found to provide near catalyst-free aqueous solutions of PHIP contrast agents. This method relies on the following steps: a) hydrogenation of a labile, lipophilic precursor of the target substrate in a hydrophobic organic solvent (*e.g.* chloroform); b) SOT; c) hydrolysis of the hyperpolarized product by means of fast reaction with an aqueous base - for instance, carboxylate sodium salts (hydrophilic) can be obtained by hydrolysis of the corresponding esters (lipophilic); d) extraction of the aqueous phase that contains the hydrophilic product, Figure 7.[79] To obtain a biocompatible pH, an acidic buffer was added.[56,80,82,219] The technique was shown to work well with PHIP-SAH[20] and has provided aqueous solution of hyperpolarized sodium [1-^{13}C]pyruvate and acetate, *e.g.*, by hydrogenating their propargylic or vinyl esters.

The LL phase extraction can be performed in any solvent-resistant container, *e.g.*, in NMR tubes or a dedicated reactor. Its efficiency depends on the level of dispersion of small droplets of the organic solution into the aqueous phase, as hydrolysis likely occurs at the LL interface. As the dispersion should happen as fast as possible, injecting heated and pressurized base solution into the organic phase was suggested (a video showing the procedure can be found in ref.[220]). Instead

of using pure hydrophobic chloroform,[221] mixtures containing some (few %) hydrophilic solvents (*i.e.*, ethanol, methanol) or toluene have been suggested[82,220] to further improve the LL mixing and hydrolysis, as well as bubbling N_2 gas through the solution.[82] Ultimately, thanks to the instability of the LL mixture, the two phases separate within a few seconds.

Notably, this approach was used for the first *in cellulo* and *in vivo* metabolic studies with PHIP-polarized pyruvate,[80,219,221] after a first demonstration of hyperpolarized [1-^{13}C]succinate (from maleic anhydride).[79] Losses of polarization during hydrolysis and phase transfer of the ester derivatives have been observed and could not be explained by T_1 relaxation alone.[157] Instead, the effect has been attributed to the presence of paramagnetic impurities derived from catalyst degradation in the organic phase and a beneficial effect on hyperpolarization has been obtained through the addition of a radical scavenger (sodium ascorbate) to the aqueous base. The concentration of the metal (rhodium) in the aqueous phase has been determined to be 30 μM.[222]

Solvents such as methanol, ethanol, and acetone mix well with water and are transferred to the aqueous phase during phase extraction. Therefore, their application in the hyperpolarization of substrates for biological use (in cells and *in vivo*) must be considered carefully, due to their toxicity, especially for methanol. Nevertheless, it must be mentioned that, even when pure hydrophobic solvents (chloroform and toluene) were used, their dissolution and ultimately the concentration in the aqueous phase is non-negligible and a cytotoxicity effect has been observed.[219] In order to solve this issue, filtration of the aqueous solution through a lipophilic resin (Tenax TA, Porous Polymer Adsorbent, 60-80 mesh, Supelco) was recently shown to lead to a reduction of the concentration of these solvents well below the concentration recommended by Environmental Protection Agencies (EPA).[69,220]

Heterogeneous Catalysts

In contrast to homogeneous catalysis, heterogeneous catalysis affords straightforward separation of the solution-state hyperpolarized hydrogenation adducts from the solid catalyst due to the insolubility of the latter. Moreover, heterogeneous catalysis is inherently compatible with continuous-flow production of HP gases and liquids. These advantages were already recognized in the initial demonstration of HET-PHIP[73] and continue to drive the development of HET-PHIP catalysts and reactor systems.

In ref.[73] silica and a polymer were functionalized with phosphine groups to chelate the Rh complex (*e.g.* Wilkinson's catalyst). The linkage proved to be resilient, but the catalysts still suffered from low stability, possible leaching into solution upon oxidation of the phosphine moieties, reduction during the reaction, and metal complex dimerization.[192] A recent article described an alternative linkage scheme, where a silica supported polymer incorporating pyridyl groups was used to tether Wilkinson's catalyst.[223] This catalyst showed better stability and resistance to leaching. Modest signal enhancements of up to 200 were reported for the hydrogenation of styrene in acetone-d$_6$.

In the quest to realize efficient, stable and robust HET-PHIP catalysts, metal-oxide-supported nanoparticle catalysts

consisting of Pt, Pd, Rh, Ru, Ir as well as bimetallic compositions (*e.g.* Pd-In)[224] and intermetallic nanoparticles (*e.g.* PtSn, Pt_3Sn)[214] with varying shapes, sizes, and support materials have been explored.[192] Most of the published solution-state HET-PHIP studies were performed using a batch reactor configuration,[214,224–227] where hydrogen is bubbled through a heated NMR tube containing the insoluble solid catalyst and the unsaturated substrate in solution. For larger catalyst particles (millimeter size), settling out of the catalyst after cessation of bubbling can occur within seconds. Under the relatively mild conditions of solution-state hydrogenation, supported metal nanoparticles were found to resist leaching. For example, after hydrogenation of 2-hydroxyethyl acrylate over 25 mg of Pt_3Sn intermetallic nanoparticles in 2 mL D_2O at 120 °C and 5.7 bar, Pt and Sn levels in the decanted solution were found to be well below 100 ppb (by mass).[214] Transfer of hyperpolarization to heteronuclei in aqueous media for biologically relevant compounds has been addressed as well.[228]

As noted above, MRI of HP ^{13}C pyruvate provides a means for detection of abnormal metabolism in malignant tumors and other pathologies. There is evidence, however, that administration of a continuous stream of the HP pyruvate over longer periods is preferable to a single large bolus for some applications.[229] Production of purified continuous-flow streams of HP pyruvate by either dissolution DNP or PHIP is challenging and has not yet been demonstrated.

Hale *et al.* recently presented a novel apparatus that allowed continuous production of hyperpolarized allyl acetate by hydrogenation of propargyl acetate with pH_2, Figure 7. The apparatus incorporated a packed-bed catalytic reactor, side-arm hydrogenation, and pH_2 membrane dissolution.[18] The polarizer continuously achieved a conversion of 30 % and ^{1}H signal enhancements up to 300 (relative to thermal equilibrium at 9.4 Tesla) were shown to be feasible. However, the polarization transfer to ^{13}C, side-arm cleavage, and transfer to the aqueous phase have yet to be addressed.

Challenges for heterogeneous catalysis include lower product concentrations and lower polarizations compared to homogeneous approaches. To solve these shortcomings, emphasis is made on improved flow reactor design as well as the rational design of catalysts to obtain higher pairwise selectivity without sacrificing yield.

Precipitation

Very recently, a scheme to purify HP molecules based on precipitation was introduced.[24,230] HP fumarate was generated in an aqueous solution using a trans-selective hydrogenation catalyst. After hydrogenation and polarization transfer, the reaction solution contained the ruthenium-based catalyst, unreacted starting material, and side products in addition to the desired HP fumarate salt. To purify the solution, acid and non-polarized fumarate were added to the solution so that fumaric acid precipitated out of the solution almost immediately.

Because fumarate precipitated very efficiently and the catalyst, starting material, and side products remained mostly dissolved, separation was easily achieved by decanting the solution. Subsequently, the solid, HP fumaric acid was re-dissolved in aqueous solution. It was important to keep the solid fumarate (from precipitation to re-dissolution) at a sufficiently high magnetic field to avoid fast relaxation in the solid state. The remaining metal concentration was found to be 16 μM after a washing procedure.[24] While this method worked well for fumarate, the generality of this approach remains an open question, and further research towards this promising approach is certainly warranted.
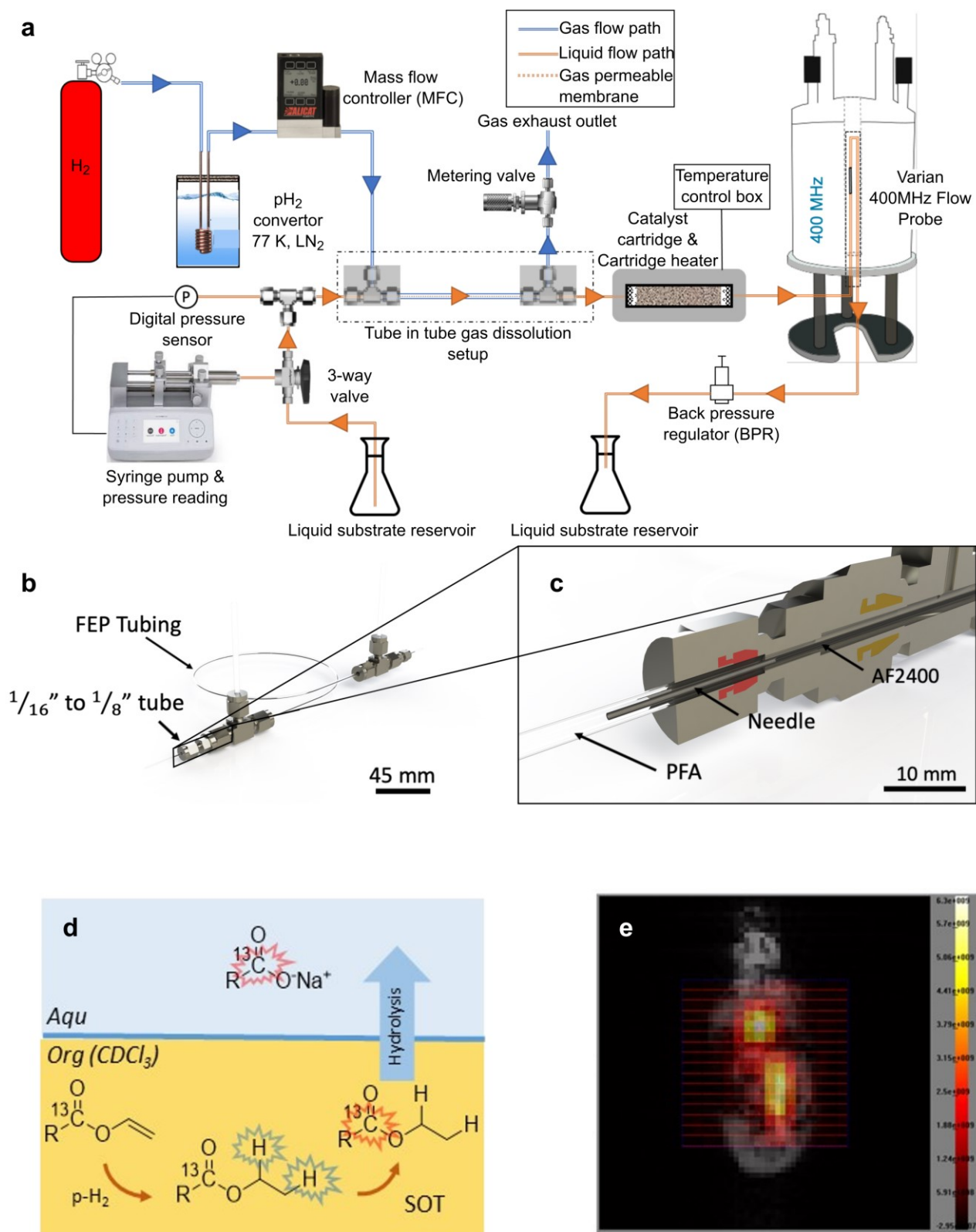
Figure 7. Upper panel: Continuous-flow liquid-state ALTADENA HET-PHIP polarizer. a) The system incorporated a packed-bed heterogeneous reactor containing a slid Rh/TiO₂ nano-rod catalyst and a tube-in-tube membrane system for bubble-free pH₂ dissolution. The liquid is drawn into the syringe from the left liquid reservoir and the 3-way valve is then changed to allow the liquid to flow through the tube-in-tube and then on to the heated catalyst cartridge. b) Rendering of the tube-in-tube device. C) Close up of the liquid inlet port showing

the PFA (clear) tubing, 316 stainless steel needle (grey), and AF2400 membrane 'inner tube' (black). Figure reproduced from Toward Continuous-Flow Hyperpolarisation of Metabolites via Heterogenous Catalysis, Side-Arm-Hydrogenation, and Membrane Dissolution of Parahydrogen, Hale, W. G.; Zhao, T. Y.; Choi, D.; Ferrer, M.-J.; Song, B.; Zhao, H.; Hagelin-Weaver, H. E.; Bowers, C. R. ChemPhysChem, Vol. 22, Issue 9 (ref 18). Copyright 2021 Wiley. **Lower panel: PHIP-SAH LL-separation (left) and HP *in vivo* ^{13}C-MRI (right).** The scheme on the left shows the LL separation of a carboxylate sodium salt in the water phase from its ester in the organic phase. HP [1-^{13}C]pyruvate obtained using this method has been applied *in vivo* for metabolic studies (right): ^{13}C-CSI image of [1-^{13}C]pyruvate overlaid with an anatomical image (^{1}H-RARE) of a healthy mouse (image acquired at 3T).

OTHER INTERESTING DEVELOPMENTS

PHIP-on-a-chip:

An emerging research area that is mainly pursued at high magnetic fields is the integration of PHIP into lab-on-a-chip devices.[18,231–234] The advantage offered by working at a microfluidic scale (*i.e.*, with sample volumes on the order of microliters) is in the much higher degree of experimental control that can be leveraged, in terms of sample contact time with pH_2, molecular diffusion, temperature and pressure. The other important benefit of microfluidic implementation of PHIP experiments is in the short transport paths (and hence time) between the point of the PHIP process occurring and signal detection. This is particularly important when nuclear spin relaxation times are short.

RASER:

Radio amplification by stimulated emission (RASER) using PHIP was recently discovered[21,235] in PASADENA and ALTADENA conditions.[22,236] RASER emission was detected at low (millitesla)[235] and high fields (tesla) and reproduced by simulations.[22] Although the RASER effect was first observed using other HP techniques,[237–239] PHIP has the advantage that the polarization can be continuously refreshed by a constant supply of pH_2 as long as substrate is not depleted. While a biomedical application of RASER was not described, newly emerged applications included observation of NMR spectra with very narrow signals,[22,235] background-free proton NMR spectroscopy,[236] and polarization transfer to other molecules via intermolecular dipole-dipole interaction.[23]

PHIP-X:

pH_2 hyperpolarization relayed via chemical exchange (PHIP-X)[26] facilitates polarization of molecules that undergo suitable proton exchange like glucose.[25,240–242] First, pH_2 is added to an intermediary molecule by homogeneous catalysis, where the polarization is then transferred to an exchanging proton. Secondly, the polarization is incorporated by the target molecule by exchange of a polarized proton from the reacted intermediary molecule. Experimentally, this process was implemented by placing a high-pressure reaction chamber in millitesla fields. Upon hydrogenation, the sample was transferred to high field NMR for detection. If necessary, the target molecule can be added after the hydrogenation to avoid interference with the hydrogenation step. Both millitesla and MFC setups appear to be well suited to host this process, which involves SOT in the intermediary and target molecule, for which the spin physics has yet to be fully elucidated.

TOWARDS CLINICAL APPLICATION

The results described above impressively demonstrate the power, versatility, and maturity of pH_2-based hyperpolarization approaches and instrumentation. Indeed, HP [1-^{13}C]pyruvate produced by hydrogenative PHIP has been recently employed to detect the response of the heart to altered metabolism in real time.[80]
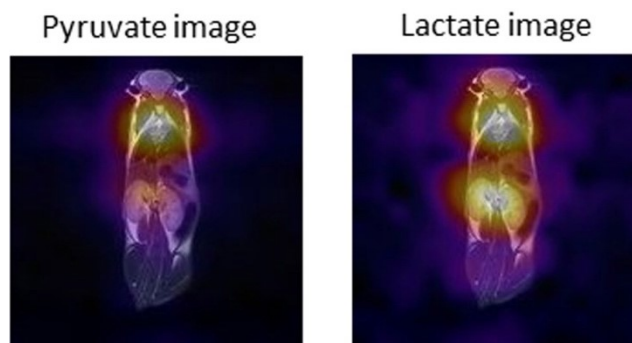

Figure 8. ^{13}C-chemical shift imaging reporting of pyruvate and lactate distribution acquired on living mice, obtained upon the injection of a dose of [1-^{13}C] pyruvate hyperpolarized using pH_2. The spatial localization of each metabolite is shown upon overlapping the ^{13}C-CSI results to the anatomical proton image (T_2 weighted fast spin echo image). Each metabolite map is scaled individually and is displayed on a fire color scale so that the region of highest metabolite signal appears white and the lowest appears black. Reprinted by permission from Nature: Sci. Rep., The 13C hyperpolarized pyruvate generated by ParaHydrogen detects the response of the heart to altered metabolism in real time, Cavallari, E.; Carrera, C.; Sorge, M.; Bonne, G.; Muchir, A.; Aime, S.; Reineri, F., Sci. Rep., Vol. 8, Issue 1 (ref 80). Copyright Nature 2018.

While preclinical imaging with PHIP agents was demonstrated in more than 15 papers since 2001, this method has not been translated to human imaging yet.[5,13,36,69,80,86,87,90,114,142–146,150]

Still, we may have reached a tipping point, as all ingredients for producing clean, aqueous solutions of interesting (not only biocompatible) agents were described in the literature. As we speak, work continues at multiple locations to make studies with PHIP-polarized agents a reality.

Let us assume that all relevant technical hurdles were to be addressed, and that there was a device that produces a clean and pure solution or solid of highly polarized contrast agent with a fast and relevant function *in vivo*. Still, there will be regulatory aspects to meet before human studies may commence. Here, much can be learned from the path taken so impressively by the DNP community.

Contrast agents are considered drugs by most regulatory bodies. As no injectable HP contrast agents are approved as

drugs (yet), the guidelines for the application and evaluation of non-approved drugs apply. On the other hand, propane (also known as E944) is approved for unlimited use in foods and is already regulated by FDA. The above regulatory requirements may vary between countries, but are likely to include

1. GMP manufacturing of ingredients by vendor or in-house – pH$_2$, catalyst, solvents, precursors
2. ISO 5 clean bench (or higher depending on regulations) preparation of ingredients on site – mixing precursor solution, pH$_2$
3. Polarization and rapid QC – measure sample concentration, temperature, pH and polarization; residual catalyst concentration, perform sterile filter integrity test.

These steps would be followed by transfer, administration by an MD or qualified person, and imaging. However, prior to injection the hyperpolarized CA should be passed through a 0.2 µm pore size filter (the integrity of the filter would need to be tested in accordance with manufacturer regulations to ensure sterility). Given the limited lifetime of hyperpolarization, the QC needs to be rapid (< 30 s) and is recommended to be performed in parallel with the sample transfer and filter integrity test to minimize the time to injection. The transfer distance will be determined by the lifetime, and long-lived samples may be transported between sites. Attempts for individual treatment of patients on a small scale may require less stringent regulations. Safety and dose escalation trials would be followed by efficacy tests.

CONCLUSIONS

pH$_2$-based hyperpolarization has come a long way since its inception in the 1980s, and the first demonstration of hyperpolarized *in vivo* ^{13}C-MRI in 2001. For hyperpolarizing small molecules in solution for *in vivo* MRI application, dDNP is currently the state-of-the-art methodology, but PHIP is beginning to emerge as a viable alternative. Arguably, there is no hyperpolarization technique that is more flexible and that offers more variants than PHIP. In addition, PHIP is inexpensive, (often) easy to implement, fast and scalable. Consequently, many applications have emerged, ranging from basic physics to chemistry and biomedicine. The latter, however, has not advanced as fast as, *e.g.*, with dDNP.

The main advantages of PHIP lie in the inherent low cost, ease of implementation, rate of hyperpolarized sample turnover, and scalability. These advantages stem mainly from the chemical nature of the technique; hyperpolarization is delivered via chemical reactions rather than requiring cryogenic cooling of the to-be-polarized substance and/or irradiation with high power microwaves, as is the case for dDNP. The chemical basis of the process unfortunately carries some drawbacks: (1) the method is limited to polarizing molecules that can be generated through hydrogenation reactions; (2) the HP solutions are contaminated with other chemicals from the reaction, and; (3) polarization levels are often only modest since the nuclear spins relax during the hyperpolarization process.

All three drawbacks are being overcome through state-of-the-art research, much of which is covered in this review: Many biologically and diagnostically promising agents are available by direct hydrogenation (SUX, FUM, TFPP, PLAC) and variants such as PHIP-SAH and PHIP-X (pyruvate, acetate,

glucose, lactate). Physicochemical methods for purifying the HP solutions through phase separation have been shown for a few PHIP-polarized metabolites, and scavenging can be used to remove the catalyst from solutions. Advances in instrumentation for hydrogenation, polarization transfer, and sample transport, have helped to improve the resulting polarization levels in PHIP-polarized molecules. PHIP seems to be a promising hyperpolarization method for preclinical MRI and *in vitro* studies where experiment turnover is high but requirements for high polarization and solution sterility/nontoxicity are lower.

Nonetheless, it remains to be seen whether PHIP has a future role to play in clinical imaging. To date no device is commercially available – not even for *in vitro* and preclinical *in vivo* studies. Over the years, some initiatives were and still are active (Amersham, Stelar, Spindynamics, Bruker, XEUS Technologies LTD, NVision), and numerous patents were filed. The technical challenges towards clinical applications are accompanied by regulatory aspects, which must be met for a use in human. Here, the contrast agents do not only need to be pure and highly polarized, but also produced effectively and compliant to GMP. The reactive nature of PHIP may pose a challenge, too. Ideally, agents must have a long enough lifetime for testing and transferring after polarization.

Although the focus of this review has largely been on producing PHIP-polarized biomolecules for *in vivo* applications, there are many more uses of PHIP. Examples include studying chemical reaction mechanisms and as a source of signal enhancement for high-resolution NMR. Advances in instrumentation have underpinned much of the method development made in recent years, and will continue to pave the way into the future. Even if PHIP (or hyperpolarization in general) would eventually turn out to be ineligible for clinics, many more applications are lurking behind the corner – the marriage of pH$_2$ and MR are far from over yet, and the best has yet to come.

AUTHOR INFORMATION

Corresponding Authors

*Andreas Schmidt (andreas.schmidt@uniklinik-freiburg.de)

*Jan-Bernd Hövener (jan.hoevener@rad.uni-kiel.de)

Author Contributions

The manuscript was written through contributions of all authors. All authors have given approval to the final version of the manuscript.

REFERENCES

(1)   Born, M.; Heisenberg, W. The Quantum Theory of Molecules. *Ann Phys-Berl. Ann Phys-Berl.* **1924**, *74* (9), 1–31.

(2)   Bowers, C. R.; Weitekamp, D. P. Transformation of Symmetrization Order to Nuclear-Spin Magnetization by Chemical Reaction and Nuclear Magnetic Resonance. *Phys. Rev. Lett.* **1986**, *57* (21), 2645–2648. https://doi.org/10.1103/PhysRevLett.57.2645.

(3)   Bowers, C. R.; Weitekamp, D. P. Parahydrogen and Synthesis Allow Dramatically Enhanced Nuclear Alignment. *J. Am. Chem. Soc.* **1987**, *109* (18), 5541–5542.

(4)   Eisenschmid, T. C.; Kirss, R. U.; Deutsch, P. P.; Hommeltoft, S. I.; Eisenberg, R.; Bargon, J.; Lawler, R. G.; Balch, A. L. Para Hydrogen Induced Polarization in Hydrogenation Reactions. *J. Am. Chem. Soc.* **1987**, *109* (26), 8089–8091.

(5)   Golman, K.; Axelsson, O.; Johannesson, H.; Mansson, S.; Olofsson, C.; Petersson, J. S. Parahydrogen-Induced Polarization in Imaging: Subsecond 13C Angiography. *Magn. Reson. Med.* **2001**, *46* (1), 1–5.

(6)   Johansson, E.; Olsson, L. e.; Månsson, S.; Petersson, J. s.; Golman, K.; Ståhlberg, F.; Wirestam, R. Perfusion Assessment with Bolus Differentiation: A Technique Applicable to Hyperpolarized Tracers. *Magn. Reson. Med.* **2004**, *52* (5), 1043–1051. https://doi.org/10.1002/mrm.20247.

(7)   Bargon, J.; Kandels, J.; Kating, P. Nuclear Magnetic Resonance Studies of Homogeneous Catalysis Using Parahydrogen: Analysis of Nuclear Singlet–Triplet Mixing as a Diagnostic Tool to Characterize Intermediates. *J. Chem. Phys.* **1993**, *98* (8), 6150–6153. https://doi.org/10.1063/1.464853.

(8)   Messerle, B. A.; Sleigh, C. J.; Partridge, M. G.; Duckett, S. B. Structure and Dynamics in Metal Phosphine Complexes Using Advanced NMR Studies with Para-Hydrogen Induced Polarisation. *J. Chem. Soc. Dalton Trans.* **1999**, No. 9, 1429–1436. https://doi.org/10.1039/A809948K.

(9)   Eills, J.; Stevanato, G.; Bengs, C.; Glöggler, S.; Elliott, S. J.; Alonso-Valdesueiro, J.; Pileio, G.; Levitt, M. H. Singlet Order Conversion and Parahydrogen-Induced Hyperpolarization of 13C Nuclei in near-Equivalent Spin Systems. *J. Magn. Reson.* **2017**, *274*, 163–172. https://doi.org/10.1016/j.jmr.2016.11.010.

(10)   Duckett, S. B.; Wood, N. J. Parahydrogen-Based NMR Methods as a Mechanistic Probe in Inorganic Chemistry. *Coord. Chem. Rev.* **2008**, *252* (21), 2278–2291. https://doi.org/10.1016/j.ccr.2008.01.028.

(11)   Nelson, S. J.; Kurhanewicz, J.; Vigneron, D. B.; Larson, P. E. Z.; Harzstark, A. L.; Ferrone, M.; Criekinge, M. van; Chang, J. W.; Bok, R.; Park, I.; Reed, G.; Carvajal, L.; Small, E. J.; Munster, P.; Weinberg, V. K.; Ardenkjaer-Larsen, J. H.; Chen, A. P.; Hurd, R. E.; Odegardstuen, L.-I.; Robb, F. J.; Tropp, J.; Murray, J. A. Metabolic Imaging of Patients with Prostate Cancer Using Hyperpolarized [1-13C]Pyruvate. *Sci. Transl. Med.* **2013**, *5* (198), 108. https://doi.org/10.1126/scitranslmed.3006070.

(12)   Ardenkjær-Larsen, J. H.; Bowen, S.; Petersen, J. R.; Rybalko, O.; Vinding, M. S.; Ullisch, M.; Nielsen, N. Chr. Cryogen-free Dissolution Dynamic Nuclear Polarization Polarizer Operating at 3.35 T, 6.70 T, and 10.1 T. *Magn. Reson. Med.* **2019**, *81* (3), 2184–2194. https://doi.org/10.1002/mrm.27537.

(13)   Hövener, J.-B.; Chekmenev, E. Y.; Harris, K. C.; Perman, W. H.; Robertson, L. W.; Ross, B. D.; Bhattacharya, P. PASADENA Hyperpolarization of 13C Biomolecules: Equipment Design and Installation. *Magn Reson Mater Phy* **2009**, *22*, 111–121.

(14)   Adams, R. W.; Aguilar, J. A.; Atkinson, K. D.; Cowley, M. J.; Elliott, P. I. P.; Duckett, S. B.; Green, G. G. R.; Khazal, I. G.; López-Serrano, J.; Williamson, D. C. Reversible Interactions with Para-Hydrogen Enhance NMR Sensitivity by Polarization Transfer. *Science* **2009**, *323* (5922), 1708–1711. https://doi.org/10.1126/science.1168877.

(15)   Barskiy, D. A.; Coffey, A. M.; Nikolaou, P.; Mikhaylov, D. M.; Goodson, B. M.; Branca, R. T.; Lu, G. J.; Shapiro, M. G.; Telkki, V.-V.; Zhivonitko,

V. V.; Koptyug, I. V.; Salnikov, O. G.; Kovtunov, K. V.; Bukhtiyarov, V. I.; Rosen, M. S.; Barlow, M. J.; Safavi, S.; Hall, I. P.; Schröder, L.; Chekmenev, E. Y. NMR Hyperpolarization Techniques of Gases. *Chem. – Eur. J.* **2017**, *23* (4), 725–751. https://doi.org/10.1002/chem.201603884.

(16) Kovtunov, K. V.; Koptyug, I. V.; Fekete, M.; Duckett, S. B.; Theis, T.; Joalland, B.; Chekmenev, E. Y. Parahydrogen-Induced Hyperpolarization of Gases. *Angew. Chem. Int. Ed.* **2020**, *59* (41), 17788–17797. https://doi.org/10.1002/anie.201915306.

(17) Hövener, J.-B.; Schwaderlapp, N.; Lickert, T.; Duckett, S. B.; Mewis, R. E.; Highton, L. A. R.; Kenny, S. M.; Green, G. G. R.; Leibfritz, D.; Korvink, J. G.; Hennig, J.; von Elverfeldt, D. A Hyperpolarized Equilibrium for Magnetic Resonance. *Nat. Commun.* **2013**, *4*, 2946. https://doi.org/10.1038/ncomms3946.

(18) Hale, W. G.; Zhao, T. Y.; Choi, D.; Ferrer, M.-J.; Song, B.; Zhao, H.; Hagelin-Weaver, H. E.; Bowers, C. R. Toward Continuous-Flow Hyperpolarisation of Metabolites via Heterogenous Catalysis, Side-Arm-Hydrogenation, and Membrane Dissolution of Parahydrogen. *ChemPhysChem* **2021**, *22* (9), 822–827. https://doi.org/10.1002/cphc.202100119.

(19) Eshuis, N.; Aspers, R. L. E. G.; van Weerdenburg, B. J. A.; Feiters, M. C.; Rutjes, F. P. J. T.; Wijmenga, S. S.; Tessari, M. 2D NMR Trace Analysis by Continuous Hyperpolarization at High Magnetic Field. *Angew. Chem. Int. Ed.* **2015**, *54* (48), 14527–14530. https://doi.org/10.1002/anie.201507831.

(20) Reineri, F.; Boi, T.; Aime, S. ParaHydrogen Induced Polarization of 13C Carboxylate Resonance in Acetate and Pyruvate. *Nat. Commun.* **2015**, *6*, 5858. https://doi.org/10.1038/ncomms6858.

(21) Appelt, S.; Kentner, A.; Lehmkuhl, S.; Blümich, B. From LASER Physics to the Para-Hydrogen Pumped RASER. *Prog. Nucl. Magn. Reson. Spectrosc.* **2019**, *114–115*, 1–32. https://doi.org/10.1016/j.pnmrs.2019.05.003.

(22) Pravdivtsev, A. N.; Sönnichsen, F. D.; Hövener, J.-B. Continuous Radio Amplification by Stimulated Emission of Radiation Using Parahydrogen Induced Polarization (PHIP-RASER) at 14 Tesla. *ChemPhysChem* **2020**, *21* (7), 667–672. https://doi.org/10.1002/cphc.201901056.

(23) Korchak, S.; Kaltschnee, L.; Dervisoglu, R.; Andreas, L.; Griesinger, C.; Glöggler, S. Spontaneous Enhancement of Magnetic Resonance Signals Using a RASER. *Angew. Chem. Int. Ed.* **2021**, *60* (38), 20984–20990. https://doi.org/10.1002/anie.202108306.

(24) Knecht, S.; Blanchard, J. W.; Barskiy, D.; Cavallari, E.; Dagys, L.; Dyke, E. V.; Tsukanov, M.; Bliemel, B.; Münnemann, K.; Aime, S.; Reineri, F.; Levitt, M. H.; Buntkowsky, G.; Pines, A.; Blümler, P.; Budker, D.; Eills, J. Rapid Hyperpolarization and Purification of the Metabolite Fumarate in Aqueous Solution. *Proc. Natl. Acad. Sci.* **2021**, *118* (13). https://doi.org/10.1073/pnas.2025383118.

(25) Roy, S. S.; Appleby, K. M.; Fear, E. J.; Duckett, S. B. SABRE-Relay: A Versatile Route to Hyperpolarization. *J. Phys. Chem. Lett.* **2018**, *9* (5), 1112–1117. https://doi.org/10.1021/acs.jpclett.7b03026.

(26) Them, K.; Ellermann, F.; Pravdivtsev, A. N.; Salnikov, O. G.; Skovpin, I. V.; Koptyug, I. V.; Herges, R.; Hövener, J.-B. Parahydrogen-Induced Polarization Relayed via Proton Exchange. *J. Am. Chem. Soc.* **2021**, *143* (34), 13694–13700. https://doi.org/10.1021/jacs.1c05254.

(27) Marshall, H.; Stewart, N. J.; Chan, H.-F.; Rao, M.; Norquay, G.; Wild, J. M. In Vivo Methods and Applications of Xenon-129 Magnetic Resonance. *Prog. Nucl. Magn. Reson. Spectrosc.* **2021**, *122*, 42–62. https://doi.org/10.1016/j.pnmrs.2020.11.002.

(28) Hoevener, J.-B.; Bär, S.; Leupold, J.; Jenne, K.; Leibfritz, D.; Hennig, J.; Duckett, S. B.; von Elverfeldt, D. A Continuous-Flow, High-Throughput, High-Pressure Parahydrogen Converter for Hyperpolarization in a Clinical Setting. *NMR Biomed.* **2013**, *26*, 124–131.

(29) Feng, B.; Coffey, A. M.; Colon, R. D.; Chekmenev, E. Y.; Waddell, K. W. A Pulsed Injection Parahydrogen Generator and Techniques for Quantifying Enrichment. *J. Magn. Reson.* **2012**, *214* (Supplement C), 258–262. https://doi.org/10.1016/j.jmr.2011.11.015.

(30) Wagner, S. Conversion Rate of Para-Hydrogen to Ortho-Hydrogen by Oxygen: Implications for PHIP Gas Storage and Utilization. *Magn. Reson. Mater. Phys. Biol. Med.* **2014**, *27* (3), 195–199. https://doi.org/10.1007/s10334-013-0399-y.

(31) Aroulanda, C.; Starovoytova, L.; Canet, D. Longitudinal Nuclear Spin Relaxation of Ortho- and Para-Hydrogen Dissolved in Organic Solvents. *J Phys Chem A* **2007**, *111* (42), 10615–10624.

(32) Buntkowsky, G.; Walaszek, B.; Adamczyk, A.; Xu, Y.; Limbach, H.-H.; Chaudret, B. Mechanism of Nuclear Spin Initiated Para -H 2 to Ortho -H 2 Conversion. *Phys. Chem. Chem. Phys.* **2006**, *8* (16), 1929–1935. https://doi.org/10.1039/B601594H.

(33) Schmidt, A. B.; Wörner, J.; Pravdivtsev, A.; Knecht, S.; Scherer, H.; Weber, S.; Hennig, J.; von Elverfeldt, D.; Hövener, J.-B. Lifetime of Parahydrogen in Aqueous Solutions and Human Blood. *ChemPhysChem* **2019**, *20* (19), 2408–2412. https://doi.org/10.1002/cphc.201900670.

(34) Kiryutin, A. S.; Sauer, G.; Yurkovskaya, A. V.; Limbach, H.-H.; Ivanov, K. L.; Buntkowsky, G. Parahydrogen Allows Ultrasensitive Indirect NMR Detection of Catalytic Hydrogen Complexes. *J. Phys. Chem. C* **2017**, *121* (18), 9879–9888. https://doi.org/10.1021/acs.jpcc.7b01056.

(35) Freeman, R.; Wittekoek, S.; Ernst, R. R. High-Resolution NMR Study of Relaxation Mechanisms in a Two-Spin System. *J. Chem. Phys.* **1970**, *52* (3), 1529–1544. https://doi.org/10.1063/1.1673164.

(36) Kadlecek, S.; Vahdat, V.; Nakayama, T.; Ng, D.; Emami, K.; Rizi, R. A Simple and Low-Cost Device for Generating Hyperpolarized Contrast Agents Using Parahydrogen. *NMR Biomed.* **2011**, *24* (8), 933–942. https://doi.org/10.1002/nbm.1757.

(37) Pravdivtsev, A. N.; Ivanov, K. L.; Kaptein, R.; Yurkovskaya, A. V. Theoretical Study of Dipolar Relaxation of Coupled Nuclear Spins at Variable Magnetic Field. *Appl. Magn. Reson.* **2013**, *44* (1), 23–39. https://doi.org/10.1007/s00723-012-0404-z.

(38) Schmidt, A. B.; Berner, S.; Schimpf, W.; Müller, C.; Lickert, T.; Schwaderlapp, N.; Knecht, S.; Skinner, J. G.; Dost, A.; Rovedo, P.; Hennig, J.; Elverfeldt, D. von; Hövener, J.-B. Liquid-State Carbon-13 Hyperpolarization Generated in an MRI System for Fast Imaging. *Nat. Commun.* **2017**, *8*, 14535. https://doi.org/10.1038/ncomms14535.

(39) Berner, S.; Schmidt, A. B.; Zimmermann, M.; Pravdivtsev, A. N.; Glöggler, S.; Hennig, J.; von Elverfeldt, D.; Hövener, J.-B. SAMBADENA Hyperpolarization of 13C-Succinate in an MRI: Singlet-Triplet Mixing Causes Polarization Loss. *ChemistryOpen* **2019**, *8* (6), 728–736. https://doi.org/10.1002/open.201900139.

(40) Natterer, J.; Bargon, J. Parahydrogen Induced Polarization. *Prog. Nucl. Magn. Reson. Spectrosc.* **1997**, *31* (4), 293–315. https://doi.org/10.1016/S0079-6565(97)00007-1.

(41) Nasibulov, E. A.; Pravdivtsev, A. N.; Yurkovskaya, A. V.; Lukzen, N. N.; Vieth, H.-M.; Ivanov, K. L. Analysis of Nutation Patterns in Fourier-Transform NMR of Non-Thermally Polarized Multispin Systems. *Z. Für Phys. Chem.* **2013**, *227* (6–7), 929–953. https://doi.org/10.1524/zpch.2013.0397.

(42) Goldman, M.; Johannesson, H. Conversion of a Proton Pair Para Order into 13C Polarization by Rf Irradiation, for Use in MRI. *Comptes Rendus Phys.* **2005**, *6*, 575–581.

(43) Torres, O.; Procacci, B.; Halse, M. E.; Adams, R. W.; Blazina, D.; Duckett, S. B.; Eguillor, B.; Green, R. A.; Perutz, R. N.; Williamson, D. C. Photochemical Pump and NMR Probe: Chemically Created NMR Coherence on a Microsecond Time Scale. *J. Am. Chem. Soc.* **2014**, *136* (28), 10124–10131. https://doi.org/10.1021/ja504732u.

(44) N. Pravdivtsev, A.; V. Yurkovskaya, A.; A. Petrov, P.; Vieth, H.-M. Coherent Evolution of Singlet Spin States in PHOTO-PHIP and M2S Experiments. *Phys. Chem. Chem. Phys.* **2017**, *19* (38), 25961–25969. https://doi.org/10.1039/C7CP04122E.

(45) Bowers, C. R. Sensitivity Enhancement Utilizing Parahydrogen. In *eMagRes*; American Cancer Society, 2007. https://doi.org/10.1002/9780470034590.emrstm0489.

(46) Bowers, C. R. Parahydrogen and Synthesis Allow Dramatically Enhanced Nuclear Alignment. phd, California Institute of Technology, 1991. https://doi.org/10.7907/R5TV-Z220.

(47) Natterer, J.; Schedletzky, O.; Barkemeyer, J.; Bargon, J.; Glaser, S. J. Investigating Catalytic Processes with Parahydrogen: Evolution of Zero-Quantum Coherence in AA′X Spin Systems. *J. Magn. Reson.* **1998**, *133* (1), 92–97. https://doi.org/10.1006/jmre.1998.1421.

(48) Berner, S.; Schmidt, A. B.; Ellermann, F.; Korchak, S.; Chekmenev, E. Y.; Glöggler, S.; Elverfeldt, D. von; Hennig, J.; Hövener, J.-B. High Field Parahydrogen Induced Polarization of Succinate and Phospholactate. *Phys. Chem. Chem. Phys.* **2021**, *23* (3), 2320–2330. https://doi.org/10.1039/D0CP06281B.

(49) Pravica, M. G.; Weitekamp, D. P. Net NMR Alignment by Adiabatic Transport of Parahydrogen Addition Products to High Magnetic Field. *Chem. Phys. Lett.* **1988**, *145* (4), 255–258. https://doi.org/10.1016/0009-2614(88)80002-2.

(50) Plaumann, M.; Bommerich, U.; Trantzschel, T.; Lego, D.; Dillenberger, S.; Sauer, G.; Bargon, J.; Buntkowsky, G.; Bernarding, J. Parahydrogen-Induced Polarization Transfer to 19F in Perfluorocarbons for 19F NMR Spectroscopy and MRI. *Chem. – Eur. J.* **2013**, *19* (20), 6334–6339. https://doi.org/10.1002/chem.201203455.

(51) Bär, S.; Lange, T.; Leibfritz, D.; Hennig, J.; von Elverfeldt, D.; Hoevener, J.-B. On the Spin Order Transfer from Parahydrogen to Another Nucleus. *J. Magn. Reson.* **2012**, *225*, 25–35.

(52) Svyatova, A.; Skovpin, I. V.; Chukanov, N. V.; Kovtunov, K. V.; Chekmenev, E. Y.; Pravdivtsev, A. N.; Hövener, J.-B.; Koptyug, I. V. 15N MRI of SLIC-SABRE Hyperpolarized 15N-Labelled Pyridine and Nicotinamide. *Chem. – Eur. J.* **2019**, *25* (36), 8465–8470. https://doi.org/10.1002/chem.201900430.

(53) Shchepin, R. V.; Coffey, A. M.; Waddell, K. W.; Chekmenev, E. Y. Parahydrogen Induced Polarization of 1-13C-Phospholactate-D2 for Biomedical Imaging with >30,000,000-Fold NMR Signal Enhancement in Water. *Anal. Chem.* **2014**, *86* (12), 5601–5605. https://doi.org/10.1021/ac500952z.

(54) Schmidt, A. B.; Brahms, A.; Ellermann, F.; Berner, S.; Hennig, J.; von Elverfeldt, D.; Herges, R.; Hövener, J.-B.; Pravdivtsev, A. N. Selectively Pulsed Spin Order Transfer Increases Parahydrogen-Induced NMR Amplification of Insensitive Nuclei and Makes Polarization Transfer More Robust. *ArXiv210904799 Phys.* **2021**.

(55) Jóhannesson, H.; Axelsson, O.; Karlsson, M. Transfer of Para-Hydrogen Spin Order into Polarization by Diabatic Field Cycling. *Comptes Rendus Phys.* **2004**, *5* (3), 315–324. https://doi.org/10.1016/j.crhy.2004.02.001.

(56) Cavallari, E.; Carrera, C.; Boi, T.; Aime, S.; Reineri, F. Effects of Magnetic Field Cycle on the Polarization Transfer from Parahydrogen to Heteronuclei through Long-Range J-Couplings. *J. Phys. Chem. B* **2015**, *119* (31), 10035–10041. https://doi.org/10.1021/acs.jpcb.5b06222.

(57) Kadlecek, S.; Emami, K.; Ishii, M.; Rizi, R. Optimal Transfer of Spin-Order between a Singlet Nuclear Pair and a Heteronucleus. *J. Magn. Reson.* **2010**, *205* (1), 9–13. https://doi.org/10.1016/j.jmr.2010.03.004.

(58) Cai, C.; Coffey, A. M.; Shchepin, R. V.; Chekmenev, E. Y.; Waddell, K. W. Efficient Transformation of Parahydrogen Spin Order into Heteronuclear

Magnetization. *J. Phys. Chem. B* **2013**, *117* (5), 1219–1224. https://doi.org/10.1021/jp3089462.

(59) Duckett, S. B.; Newell, C. L.; Eisenberg, R. More than INEPT: Parahydrogen and INEPT + Give Unprecedented Resonance Enhancement to Carbon-13 by Direct Proton Polarization Transfer. *J. Am. Chem. Soc.* **1993**, *115* (3), 1156–1157. https://doi.org/10.1021/ja00056a054.

(60) Haake, M.; Natterer, J.; Bargon, J. Efficient NMR Pulse Sequences to Transfer the Parahydrogen-Induced Polarization to Hetero Nuclei. *J Am Chem Soc* **1996**, *118* (86), 88–91.

(61) Stevanato, G. Alternating Delays Achieve Polarization Transfer (ADAPT) to Heteronuclei in PHIP Experiments. *J. Magn. Reson.* **2017**, *274*, 148–162. https://doi.org/10.1016/j.jmr.2016.10.009.

(62) Korchak, S.; Yang, S.; Mamone, S.; Glöggler, S. Pulsed Magnetic Resonance to Signal-Enhance Metabolites within Seconds by Utilizing Para-Hydrogen. *ChemistryOpen* **2018**, *7* (5), 344–348. https://doi.org/10.1002/open.201800024.

(63) Pravdivtsev, A. N.; Kozinenko, V. P.; Hövener, J.-B. Only Para-Hydrogen Spectroscopy (OPSY) Revisited: In-Phase Spectra for Chemical Analysis and Imaging. *J. Phys. Chem. A* **2018**, *122* (45), 8948–8956. https://doi.org/10.1021/acs.jpca.8b07459.

(64) Stevanato, G.; Eills, J.; Bengs, C.; Pileio, G. A Pulse Sequence for Singlet to Heteronuclear Magnetization Transfer: S2hM. *J. Magn. Reson.* **2017**, *277*, 169–178. https://doi.org/10.1016/j.jmr.2017.03.002.

(65) Pravdivtsev, A. N.; Hövener, J.-B. Coherent Polarization Transfer in Chemically Exchanging Systems. *Phys. Chem. Chem. Phys.* **2020**, *22* (16), 8963–8972. https://doi.org/10.1039/C9CP06873B.

(66) Hogben, H. J.; Krzystyniak, M.; Charnock, G. T. P.; Hore, P. J.; Kuprov, I. Spinach – A Software Library for Simulation of Spin Dynamics in Large Spin Systems. *J. Magn. Reson.* **2011**, *208* (2), 179–194. https://doi.org/10.1016/j.jmr.2010.11.008.

(67) Smith, S. A.; Levante, T. O.; Meier, B. H.; Ernst, R. R. Computer Simulations in Magnetic Resonance. An Object-Oriented Programming Approach. *J. Magn. Reson. A* **1994**, *106* (1), 75–105. https://doi.org/10.1006/jmra.1994.1008.

(68) Bengs, C.; Levitt, M. H. SpinDynamica: Symbolic and Numerical Magnetic Resonance in a Mathematica Environment. *Magn. Reson. Chem.* **2018**, *56* (6), 374–414. https://doi.org/10.1002/mrc.4642.

(69) Bhattacharya, P.; Harris, K.; Lin, A. P.; Mansson, M.; Norton, V. A.; Perman, W. H.; Weitekamp, D. P.; Ross, B. D. Ultra-Fast Three Dimensional Imaging of Hyperpolarized 13C in Vivo. *Magn. Reson. Mater. Phys. Biol. Med.* **2005**, *18* (5), 245–256. https://doi.org/10.1007/s10334-005-0007-x.

(70) Skovpin, I. V.; Zhivonitko, V. V.; Koptyug, I. V. Parahydrogen-Induced Polarization in Heterogeneous Hydrogenations over Silica-Immobilized Rh Complexes. *Appl. Magn. Reson.* **2011**, *41* (2), 393–410. https://doi.org/10.1007/s00723-011-0255-z.

(71) Kovtunov, K. V.; Zhivonitko, V. V.; Corma, A.; Koptyug, I. V. Parahydrogen-Induced Polarization in Heterogeneous Hydrogenations Catalyzed by an Immobilized Au(III) Complex. *J. Phys. Chem. Lett.* **2010**, *1* (11), 1705–1708. https://doi.org/10.1021/jz100391j.

(72) Abdulhussain, S.; Breitzke, H.; Ratajczyk, T.; Grünberg, A.; Srour, M.; Arnaut, D.; Weidler, H.; Kunz, U.; Kleebe, H. J.; Bommerich, U.; Bernarding, J.; Gutmann, T.; Buntkowsky, G. Synthesis, Solid-State NMR Characterization, and Application for Hydrogenation Reactions of a Novel Wilkinson's-Type Immobilized Catalyst. *Chem. – Eur. J.* **2014**, *20* (4), 1159–1166. https://doi.org/10.1002/chem.201303020.

(73) Koptyug, I. V.; Kovtunov, K. V.; Burt, S. R.; Anwar, M. S.; Hilty, C.; Han, S.-I.; Pines, A.; Sagdeev, R. Z. Para-Hydrogen-Induced Polarization in Heterogeneous Hydrogenation Reactions. *J. Am. Chem. Soc.* **2007**, *129* (17), 5580–5586. https://doi.org/10.1021/ja068653o.

(74) Kovtunov, K. V.; Beck, I. E.; Bukhtiyarov, V. I.; Koptyug, I. V. Observation of Parahydrogen-Induced Polarization in Heterogeneous Hydrogenation on Supported Metal Catalysts. *Angew. Chem. Int. Ed.* **2008**, *47* (8), 1492–1495. https://doi.org/10.1002/anie.200704881.

(75) Glöggler, S.; Grunfeld, A. M.; Ertas, Y. N.; McCormick, J.; Wagner, S.; Schleker, P. P. M.; Bouchard, L.-S. A Nanoparticle Catalyst for Heterogeneous Phase Para-Hydrogen-Induced Polarization in Water. *Angew. Chem. Int. Ed Engl.* **2015**, *54* (8), 2452–2456. https://doi.org/10.1002/anie.201409027.

(76) V. Kovtunov, K.; A. Barskiy, D.; G. Salnikov, O.; V. Shchepin, R.; M. Coffey, A.; M. Kovtunova, L.; I. Bukhtiyarov, V.; V. Koptyug, I.; Y. Chekmenev, E. Toward Production of Pure 13 C Hyperpolarized Metabolites Using Heterogeneous Parahydrogen-Induced Polarization of Ethyl[1- 13 C]Acetate. *RSC Adv.* **2016**, *6* (74), 69728–69732. https://doi.org/10.1039/C6RA15808K.

(77) Kaltschnee, L.; Jagtap, A. P.; McCormick, J.; Wagner, S.; Bouchard, L.-S.; Utz, M.; Griesinger, C.; Glöggler, S. Hyperpolarization of Amino Acids in Water Utilizing Parahydrogen on a Rhodium Nanocatalyst. *Chem. Weinh. Bergstr. Ger.* **2019**, *25* (47), 11031–11035. https://doi.org/10.1002/chem.201902878.

(78) Jagtap, A. P.; Kaltschnee, L.; Glöggler, S. Hyperpolarization of 15N-Pyridinium and 15N-Aniline Derivatives by Using Parahydrogen: New Opportunities to Store Nuclear Spin Polarization in Aqueous Media. *Chem. Sci.* **2019**, *10* (37), 8577–8582. https://doi.org/10.1039/c9sc02970b.

(79) Reineri, F.; Viale, A.; Ellena, S.; Boi, T.; Daniele, V.; Gobetto, R.; Aime, S. Use of Labile Precursors for the Generation of Hyperpolarized Molecules from Hydrogenation with Parahydrogen and Aqueous-Phase Extraction. *Angew. Chem. Int. Ed.* **2011**, *50*

(32), 7350–7353. https://doi.org/10.1002/anie.201101359.

(80) Cavallari, E.; Carrera, C.; Sorge, M.; Bonne, G.; Muchir, A.; Aime, S.; Reineri, F. The 13 C Hyperpolarized Pyruvate Generated by ParaHydrogen Detects the Response of the Heart to Altered Metabolism in Real Time. *Sci. Rep.* **2018**, *8* (1), 8366. https://doi.org/10.1038/s41598-018-26583-2.

(81) Barskiy, D. A.; Ke, L. A.; Li, X.; Stevenson, V.; Widarman, N.; Zhang, H.; Truxal, A.; Pines, A. Rapid Catalyst Capture Enables Metal-Free Para-Hydrogen-Based Hyperpolarized Contrast Agents. *J. Phys. Chem. Lett.* **2018**, *9* (11), 2721–2724. https://doi.org/10.1021/acs.jpclett.8b01007.

(82) Dagys, L.; Jagtap, A. P.; Korchak, S.; Mamone, S.; Saul, P.; Levitt, M. H.; Glöggler, S. Nuclear Hyperpolarization of (1-13C)-Pyruvate in Aqueous Solution by Proton-Relayed Side-Arm Hydrogenation. *Analyst* **2021**, *146* (5), 1772–1778. https://doi.org/10.1039/D0AN02389B.

(83) Goldman, M.; Johannesson, H.; Axelsson, O.; Karlsson, M. Design and Implementation of 13C Hyper Polarization from Para-Hydrogen, for New MRI Contrast Agents. *Comtes Rendus Chim.* **2006**, *9*, 357–363.

(84) Goldman, M.; Axelsson, O.; Johannesson, H.; Ardenkjaer-Larsen, J. Method and Apparatus for Producing Contrast Agents for Magnetic Resonance Imaging. US20060127313A1, June 15, 2006.

(85) Waddell, K. W.; Coffey, A. M.; Chekmenev, E. Y. In Situ Detection of PHIP at 48 MT: Demonstration Using a Centrally Controlled Polarizer. *J. Am. Chem. Soc.* **2011**, *133* (1), 97–101. https://doi.org/10.1021/ja108529m.

(86) Coffey, A. M.; Shchepin, R. V.; Truong, M. L.; Wilkens, K.; Pham, W.; Chekmenev, E. Y. Open-Source Automated Parahydrogen Hyperpolarizer for Molecular Imaging Using 13C Metabolic Contrast Agents. *Anal. Chem.* **2016**, *88*, 8279–8288.

(87) Coffey, A. M.; Shchepin, R. V.; Feng, B.; Colon, R. D.; Wilkens, K.; Waddell, K. W.; Chekmenev, E. Y. A Pulse Programmable Parahydrogen Polarizer Using a Tunable Electromagnet and Dual Channel NMR Spectrometer. *J. Magn. Reson.* **2017**, *284* (Supplement C), 115–124. https://doi.org/10.1016/j.jmr.2017.09.013.

(88) Joalland, B.; Schmidt, A. B.; Kabir, M. S. H.; Chukanov, N. V.; Kovtunov, K. V.; Koptyug, I. V.; Hennig, J.; Hövener, J.-B.; Chekmenev, E. Y. Pulse-Programmable Magnetic Field Sweeping of Parahydrogen-Induced Polarization by Side Arm Hydrogenation. *Anal. Chem.* **2020**, *92* (1), 1340–1345. https://doi.org/10.1021/acs.analchem.9b04501.

(89) Hövener, J.-B.; Chekmenev, E. Y.; Harris, K. C.; Perman, W. H.; Tran, T. T.; Ross, B. D.; Bhattacharya, P. Quality Assurance of PASADENA Hyperpolarization for 13C Biomolecules. *Magn Reson Mater Phy* **2009**, *22*, 123–134.

(90) Schmidt, A. B.; Berner, S.; Braig, M.; Zimmermann, M.; Hennig, J.; Elverfeldt, D. von; Hövener, J.-B. In Vivo 13C-MRI Using SAMBADENA. *PLOS ONE* **2018**, *13* (7), e0200141. https://doi.org/10.1371/journal.pone.0200141.

(91) Agraz, J.; Grunfeld, A. M.; Cunningham, K.; Pozos, R.; Li, D.; Wagner, S. PHIP Instrumentation Pinch Valve System for Sample Delivery, Process and Collection. *Adv. Biomed. Sci. Eng.* **2014**, *1* (1), 8–18.

(92) Borowiak, R.; Schwaderlapp, N.; Huethe, F.; Lickert, T.; Fischer, E.; Baer, S.; Hennig, J.; Elverfeldt, D. v.; Hoevener, J. B. A Battery-Driven, Low-Field NMR Unit for Thermally and Hyperpolarized Samples. *Magn. Reson. Mater. Phys. Biol. Med.* **2013**, *26* (5), 491–499. https://doi.org/10.1007/s10334-013-0366-7.

(93) Coffey, A. M.; Shchepin, R. V.; Wilkens, K.; Waddell, K. W.; Chekmenev, E. Y. A Large Volume Double Channel 1H–X RF Probe for Hyperpolarized Magnetic Resonance at 0.0475T. *J. Magn. Reson.* **2012**, *220*, 94–101. https://doi.org/10.1016/j.jmr.2012.04.012.

(94) Kiryutin, A. S.; Sauer, G.; Hadjiali, S.; Yurkovskaya, A. V.; Breitzke, H.; Buntkowsky, G. A Highly Versatile Automatized Setup for Quantitative Measurements of PHIP Enhancements. *J. Magn. Reson.* **2017**, *285* (Supplement C), 26–36. https://doi.org/10.1016/j.jmr.2017.10.007.

(95) Hövener, J.-B.; Schwaderlapp, N.; Borowiak, R.; Lickert, T.; Duckett, S. B.; Mewis, R. E.; Adams, R. W.; Burns, M. J.; Highton, L. A. R.; Green, G. G. R.; Olaru, A.; Hennig, J.; von Elverfeldt, D. Toward Biocompatible Nuclear Hyperpolarization Using Signal Amplification by Reversible Exchange: Quantitative in Situ Spectroscopy and High-Field Imaging. *Anal. Chem.* **2014**, *86* (3), 1767–1774. https://doi.org/10.1021/ac403653q.

(96) Agraz, J.; Grunfeld, A. M.; Li, D.; Cunningham, K.; Willey, C.; Pozos, R.; Wagner, S. LabVIEW-Based Control Software for Para-Hydrogen Induced Polarization Instrumentation. *Rev. Sci. Instrum.* **2014**, *85* (044705).

(97) Ellermann, F.; Pravdivtsev, A.; Hövener, J.-B. Open-Source, Partially 3D-Printed, High-Pressure (50-Bar) Liquid-Nitrogen-Cooled Parahydrogen Generator. *Magn. Reson.* **2021**, *2* (1), 49–62. https://doi.org/10.5194/mr-2-49-2021.

(98) Juarez, A. M.; Cubric, D.; King, G. C. A Compact Catalytic Converter for the Production of Para-Hydrogen. *Meas. Sci. Technol.* **2002**, *13* (5), N52–N55. https://doi.org/10/fc82nq.

(99) Sullivan, N. S.; Zhou, D.; Edwards, C. M. Precise and Efficient in Situ Ortho — Para-Hydrogen Converter. *Cryogenics* **1990**, *30* (8), 734–735. https://doi.org/10.1016/0011-2275(90)90240-D.

(100) Hövener, J.-B.; Bär, S.; Leupold, J.; Jenne, K.; Leibfritz, D.; Hennig, J.; Duckett, S. B.; von Elverfeldt, D. A Continuous-Flow, High-Throughput, High-Pressure Parahydrogen Converter for Hyperpolarization in a Clinical Setting. *NMR Biomed.* **2013**, *26* (2), 124–131. https://doi.org/10.1002/nbm.2827.

(101) Meier, B.; Dumez, J.-N.; Stevanato, G.; Hill-Cousins, J. T.; Roy, S. S.; Håkansson, P.; Mamone, S.; Brown, R. C. D.; Pileio, G.; Levitt, M. H. Long-Lived Nuclear Spin States in Methyl Groups and Quantum-Rotor-Induced Polarization. *J. Am. Chem. Soc.* **2013**, *135* (50), 18746–18749. https://doi.org/10.1021/ja410432f.

(102) Birchall, J. R.; Coffey, A. M.; Goodson, B. M.; Chekmenev, E. Y. High-Pressure Clinical-Scale 87% Parahydrogen Generator. *Anal. Chem.* **2020**, *92* (23), 15280–15284. https://doi.org/10.1021/acs.analchem.0c03358.

(103) Sundararajan, K.; Sankaran, K.; Ramanathan, N.; Gopi, R. Production and Characterization of Para-Hydrogen Gas for Matrix Isolation Infrared Spectroscopy. *J. Mol. Struct.* **2016**, *1117*, 181–191. https://doi.org/10.1016/j.molstruc.2016.03.068.

(104) Nantogma, S.; Joalland, B.; Wilkens, K.; Chekmenev, E. Y. Clinical-Scale Production of Nearly Pure (>98.5%) Parahydrogen and Quantification by Benchtop NMR Spectroscopy. *Anal. Chem.* **2021**, *93* (7), 3594–3601. https://doi.org/10.1021/acs.analchem.0c05129.

(105) Du, Y.; Zhou, R.; Ferrer, M.-J.; Chen, M.; Graham, J.; Malphurs, B.; Labbe, G.; Huang, W.; Bowers, C. R. An Inexpensive Apparatus for up to 97% Continuous-Flow Parahydrogen Enrichment Using Liquid Helium. *J. Magn. Reson.* **2020**, *321*, 106869. https://doi.org/10.1016/j.jmr.2020.106869.

(106) Buckenmaier, K.; Scheffler, K.; Plaumann, M.; Fehling, P.; Bernarding, J.; Rudolph, M.; Back, C.; Koelle, D.; Kleiner, R.; Hövener, J.; Pravdivtsev, A. N. Multiple Quantum Coherences Hyperpolarized at Ultra-Low Fields. *Chemphyschem* **2019**, *20* (21), 2823–2829. https://doi.org/10.1002/cphc.201900757.

(107) Kiryutin, A. S.; Pravdivtsev, A. N.; Ivanov, K. L.; Grishin, Y. A.; Vieth, H.-M.; Yurkovskaya, A. V. A Fast Field-Cycling Device for High-Resolution NMR: Design and Application to Spin Relaxation and Hyperpolarization Experiments. *J. Magn. Reson.* **2016**, *263*, 79–91. https://doi.org/10.1016/j.jmr.2015.11.017.

(108) Jeong, K.; Min, S.; Chae, H.; Namgoong, S. K. Detecting Low Concentrations of Unsaturated C—C Bonds by Parahydrogen-Induced Polarization Using an Efficient Home-Built Parahydrogen Generator. *Magn. Reson. Chem.* **2018**, *56* (11), 1089–1093. https://doi.org/10.1002/mrc.4756.

(109) Gamliel, A.; Allouche-Arnon, H.; Nalbandian, R.; Barzilay, C. M.; Gomori, J. M.; Katz-Brull, R. An Apparatus for Production of Isotopically and Spin-Enriched Hydrogen for Induced Polarization Studies. *Appl. Magn. Reson.* **2010**, *39* (4), 329–345. https://doi.org/10.1007/s00723-010-0161-9.

(110) Parrott, A. J.; Dallin, P.; Andrews, J.; Richardson, P. M.; Semenova, O.; Halse, M. E.; Duckett, S. B.; Nordon, A. Quantitative In Situ Monitoring of Parahydrogen Fraction Using Raman Spectroscopy. *Appl. Spectrosc.* **2019**, *73* (1), 88–97. https://doi.org/10.1177/0003702818798644.

(111) Chapman, B.; Joalland, B.; Meersman, C.; Ettedgui, J.; Swenson, R. E.; Krishna, M. C.; Nikolaou, P.; Kovtunov, K. V.; Salnikov, O. G.; Koptyug, I. V.; Gemeinhardt, M. E.; Goodson, B. M.; Shchepin, R. V.; Chekmenev, E. Y. Low-Cost High-Pressure Clinical-Scale 50% Parahydrogen Generator Using Liquid Nitrogen at 77 K. *Anal. Chem.* **2021**, *93* (24), 8476–8483. https://doi.org/10.1021/acs.analchem.1c00716.

(112) Mhaske, Y.; Sutter, E.; Mahoney, C.; Daley, J.; Whiting, N. 65% Parahydrogen from a Liquid Nitrogen Cooled Generator. In *PERM*; Online, 2021.

(113) Hövener, J.-B.; Pravdivtsev, A. N.; Kidd, B.; Bowers, C. R.; Glöggler, S.; Kovtunov, K. V.; Plaumann, M.; Katz-Brull, R.; Buckenmaier, K.; Jerschow, A.; Reineri, F.; Theis, T.; Shchepin, R. V.; Wagner, S.; Bhattacharya, P.; Zacharias, N. M.; Chekmenev, E. Y. Parahydrogen-Based Hyperpolarization for Biomedicine. *Angew. Chem. Int. Ed.* **2018**, *57* (35), 11140–11162. https://doi.org/10.1002/anie.201711842.

(114) Stewart, N. J.; Nakano, H.; Sugai, S.; Tomohiro, M.; Kase, Y.; Uchio, Y.; Yamaguchi, T.; Matsuo, Y.; Naganuma, T.; Takeda, N.; Nishimura, I.; Hirata, H.; Hashimoto, T.; Matsumoto, S. Hyperpolarized 13C Magnetic Resonance Imaging of Fumarate Metabolism by Parahydrogen-Induced Polarization: A Proof-of-Concept in Vivo Study. *ChemPhysChem* **2021**, *22* (10), 915–923. https://doi.org/10.1002/cphc.202001038.

(115) Sengstschmid, H.; Freeman, R.; Barkemeyer, J.; Bargon, J. A New Excitation Sequence to Observe the PASADENA Effect. *J. Magn. Reson. A* **1996**, *120* (2), 249–257. https://doi.org/10.1006/jmra.1996.0121.

(116) Kiryutin, A. S.; Ivanov, K. L.; Yurkovskaya, A. V.; Vieth, H.-M.; Lukzen, N. N. Manipulating Spin Hyper-Polarization by Means of Adiabatic Switching of a Spin-Locking RF-Field. *Phys. Chem. Chem. Phys.* **2013**, *15* (34), 14248–14255. https://doi.org/10.1039/C3CP52061G.

(117) Pravdivtsev, A. N.; Sönnichsen, F.; Hövener, J.-B. OnlyParahydrogen SpectrosopY (OPSY) Pulse Sequences – One Does Not Fit All. *J. Magn. Reson.* **2018**, *297*, 86–95. https://doi.org/10.1016/j.jmr.2018.10.006.

(118) Pravdivtsev, A. N.; Ivanov, K. L.; Yurkovskaya, A. V.; Vieth, H.-M.; Sagdeev, R. Z. New Pulse Sequence for Robust Filtering of Hyperpolarized Multiplet Spin Order. *Dokl. Phys. Chem.* **2015**, *465* (1), 267–269. https://doi.org/10.1134/S0012501615110044.

(119) Korchak, S.; Emondts, M.; Mamone, S.; Blümich, B.; Glöggler, S. Production of Highly Concentrated and Hyperpolarized Metabolites within Seconds in High and Low Magnetic Fields. *Phys. Chem. Chem. Phys.* **2019**, *21* (41), 22849–22856. https://doi.org/10.1039/C9CP05227E.

(120) Sørensen, O. W.; Ernst, R. R. Elimination of Spectral Distortion in Polarization Transfer Experiments. Improvements and Comparison of Techniques. *J. Magn. Reson. 1969* **1983**, *51* (3), 477–489. https://doi.org/10.1016/0022-2364(83)90300-1.

(121) Barkemeyer, J.; Bargon, J.; Sengstschmid, H.; Freeman, R. Heteronuclear Polarization Transfer Using Selective Pulses during Hydrogenation with Parahydrogen. *J. Magn. Reson. A* **1996**, *120* (1), 129–132. https://doi.org/10.1006/jmra.1996.0109.

(122) Pravdivtsev, A. N.; Ellermann, F.; Hövener, J.-B. Selective Excitation Doubles the Transfer of Parahydrogen-Induced Polarization to Heteronuclei. *Phys. Chem. Chem. Phys.* **2021**, *23* (26), 14146–14150. https://doi.org/10.1039/D1CP01891D.

(123) Stewart, N. J.; Kumeta, H.; Tomohiro, M.; Hashimoto, T.; Hatae, N.; Matsumoto, S. Long-Range Heteronuclear J-Coupling Constants in Esters: Implications for 13C Metabolic MRI by Side-Arm Parahydrogen-Induced Polarization. *J. Magn. Reson.* **2018**, *296*, 85–92. https://doi.org/10.1016/j.jmr.2018.08.009.

(124) Pravdivtsev, A. N.; Yurkovskaya, A. V.; Lukzen, N. N.; Ivanov, K. L.; Vieth, H.-M. Highly Efficient Polarization of Spin-1/2 Insensitive NMR Nuclei by Adiabatic Passage through Level Anticrossings. *J. Phys. Chem. Lett.* **2014**, *5* (19), 3421–3426. https://doi.org/10.1021/jz501754j.

(125) Rodin, B. A.; Kozinenko, V. P.; Kiryutin, A. S.; Yurkovskaya, A. V.; Eills, J.; Ivanov, K. L. Constant-Adiabaticity Pulse Schemes for Manipulating Singlet Order in 3-Spin Systems with Weak Magnetic Non-Equivalence. *J. Magn. Reson.* **2021**, *327*, 106978. https://doi.org/10.1016/j.jmr.2021.106978.

(126) Kozinenko, V. P.; Kiryutin, A. S.; Yurkovskaya, A. V.; Ivanov, K. L. Polarization of Low-γ Nuclei by Transferring Spin Order of Parahydrogen at High Magnetic Fields. *J. Magn. Reson.* **2019**, *309*, 106594. https://doi.org/10.1016/j.jmr.2019.106594.

(127) Korchak, S.; Mamone, S.; Glöggler, S. Over 50 % 1H and 13C Polarization for Generating Hyperpolarized Metabolites—A Para-Hydrogen Approach. *ChemistryOpen* **2018**, *7* (9), 672–676. https://doi.org/10.1002/open.201800086.

(128) Svyatova, A.; Kozinenko, V. P.; Chukanov, N. V.; Burueva, D. B.; Chekmenev, E. Y.; Chen, Y.-W.; Hwang, D. W.; Kovtunov, K. V.; Koptyug, I. V. PHIP Hyperpolarized [1-13C]Pyruvate and [1-13C]Acetate Esters via PH-INEPT Polarization Transfer Monitored by 13C NMR and MRI. *Sci. Rep.* **2021**, *11* (1), 5646. https://doi.org/10.1038/s41598-021-85136-2.

(129) Schmidt, A. B. Liquid-State Nuclear Hyperpolarization without a Polarizer: Synthesis amid the Magnet Bore Allows a Dramatically Enhanced Nuclear Alignment. PhD Thesis, Albert-Ludwigs-Universität, Freiburg im Breisgau, 2020.

(130) Korchak, S.; Jagtap, A. P.; Glöggler, S. Signal-Enhanced Real-Time Magnetic Resonance of Enzymatic Reactions at Millitesla Fields. *Chem. Sci.* **2021**, *12* (1), 314–319. https://doi.org/10.1039/D0SC04884D.

(131) Lippens, G.; Dhalluin, C.; Wieruszeski, J. M. Use of a Water Flip-Back Pulse in the Homonuclear NOESY Experiment. *J. Biomol. NMR* **1995**, *5* (3), 327–331. https://doi.org/10.1007/BF00211762.

(132) Sklenar, V. Suppression of Radiation Damping in Multidimensional NMR Experiments Using Magnetic Field Gradients. *J. Magn. Reson. A* **1995**, *114* (1), 132–135. https://doi.org/10.1006/jmra.1995.1119.

(133) Price, W. S.; Wälchli, M. NMR Diffusion Measurements of Strong Signals: The PGSE-Q-Switch Experiment. *Magn. Reson. Chem.* **2002**, *40* (13), S128–S132. https://doi.org/10.1002/mrc.1113.

(134) de Maissin, H.; Berner, S.; Ivantaev, V.; Hoevener, J.-B.; Hennig, J.; von Elverfeldt, D.; Schmidt, A. B. Dramatic Effect of Pulse Length and Bandwidth on the Efficiency of Pulsed Spin-Order-Transfer Sequences at High Field. In *Proc. Intl. Soc. Mag. Reson. Med. 29*; Online, 2021; p 3805.

(135) Ivantaev, V.; Berner, S.; de Maissin, H.; Hoevener, J.-B.; Hennig, J.; von Elverfeldt, D.; Kiselev, V.; Schmidt, A. B. Molecular Translation in Inhomogeneous Field Can Dramatically Reduce the Efficiency of Spin-Order Transfer at High Field. In *Proc. Intl. Soc. Mag. Reson. Med. 29*; Online, 2021; p 3798.

(136) Golman, K.; Olsson, L. E.; Axelsson, O.; Månsson, S.; Karlsson, M.; Petersson, J. S. Molecular Imaging Using Hyperpolarized 13C. *Br. J. Radiol.* **2003**, *76* (suppl_2), S118–S127. https://doi.org/10.1259/bjr/26631666.

(137) Goldman, M.; Jóhannesson, H.; Axelsson, O.; Karlsson, M. Hyperpolarization of 13C through Order Transfer from Parahydrogen: A New Contrast Agent for MRI. *Magn. Reson. Imaging* **2005**, *23* (2), 153–157. https://doi.org/10.1016/j.mri.2004.11.031.

(138) Shchepin, R. V.; Coffey, A. M.; Waddell, K. W.; Chekmenev, E. Y. Parahydrogen-Induced Polarization with a Rh-Based Monodentate Ligand in Water. *J. Phys. Chem. Lett.* **2012**, *3* (22), 3281–3285. https://doi.org/10.1021/jz301389r.

(139) Goodson, B. M.; Whiting, N.; Coffey, A. M.; Nikolaou, P.; Shi, F.; Gust, B. M.; Gemeinhardt, M. E.; Shchepin, R. V.; Skinner, J. G.; Birchall, J. R.; Barlow, M. J.; Chekmenev, E. Y. Hyperpolarization Methods for MRS. *eMagRes* **2015**, *4* (4). https://doi.org/10.1002/9780470034590.emrstm1457.

(140) Schmidt, A. B.; Andrews, D. L.; Rohrbach, A.; Gohn-Kreuz, C.; Shatokhin, V. N.; Kiselev, V. G.; Hennig, J.; von Elverfeldt, D.; Hövener, J.-B. Do Twisted Laser Beams Evoke Nuclear Hyperpolarization? *J. Magn. Reson.* **2016**, *268*, 58–67. https://doi.org/10.1016/j.jmr.2016.04.015.

(141) Shchepin, R. V.; Coffey, A. M.; Waddell, K. W.; Chekmenev, E. Y. PASADENA Hyperpolarized 13C Phospholactate. *J. Am. Chem. Soc.* **2012**, *134* (9), 3957–3960. https://doi.org/10.1021/ja210639c.

(142) Bhattacharya, P.; Chekmenev, E. Y.; Perman, W. H.; Harris, K. C.; Lin, A. P.; Norton, V. A.; Tan, C. T.; Ross, B. D.; Weitekamp, D. P. Towards Hyperpolarized 13C-Succinate Imaging of Brain Cancer. *J. Magn. Reson.* **2007**, *186* (1), 150–155. https://doi.org/10.1016/j.jmr.2007.01.017.

(143) Bhattacharya, P.; Chekmenev, E. Y.; Reynolds, W. F.; Wagner, S.; Zacharias, N.; Chan, H. R.; Bünger, R.; Ross, B. D. Parahydrogen-induced Polarization (PHIP) Hyperpolarized MR Receptor Imaging in Vivo: A Pilot Study of 13C Imaging of Atheroma in Mice. *NMR Biomed.* **2011**, *24* (8), 1023–1028. https://doi.org/10.1002/nbm.1717.

(144) Perman, W. H.; Bhattacharya, P.; Leupold, J.; Lin, A. P.; Harris, K. C.; Norton, V. A.; Hövener, J.-B.; Ross, B. D. Fast Volumetric Spatial-Spectral MR Imaging of Hyperpolarized 13C-Labeled Compounds Using Multiple Echo 3D BSSFP. *Magn. Reson. Imaging* **2010**, *28* (4), 459–465. https://doi.org/10.1016/j.mri.2009.12.003.

(145) Zacharias, N. M.; Chan, H. R.; Sailasuta, N.; Ross, B. D.; Bhattacharya, P. Real-Time Molecular Imaging of Tricarboxylic Acid Cycle Metabolism in Vivo by Hyperpolarized 1-13C Diethyl Succinate. *J. Am. Chem. Soc.* **2012**, *134* (2), 934–943. https://doi.org/10.1021/ja2040865.

(146) Zacharias, N. M.; McCullough, C. R.; Wagner, S.; Sailasuta, N.; Chan, H. R.; Lee, Y.; Hu, J.; Perman, W. H.; Henneberg, C.; Ross, B. D.; Bhattacharya, P. Towards Real-Time Metabolic Profiling of Cancer with Hyperpolarized Succinate. *J. Mol. Imaging Dyn.* **2016**, *6* (1), 123. https://doi.org/10.4172/2155-9937.1000123.

(147) Coffey, A. M.; Feldman, M. A.; Shchepin, R. V.; Barskiy, D. A.; Truong, M. L.; Pham, W.; Chekmenev, E. Y. High-Resolution Hyperpolarized in Vivo Metabolic 13C Spectroscopy at Low Magnetic Field (48.7mT) Following Murine Tail-Vein Injection. *J. Magn. Reson.* **2017**, *281* (Supplement C), 246–252. https://doi.org/10.1016/j.jmr.2017.06.009.

(148) Salnikov, O. G.; Shchepin, R. V.; Chukanov, N. V.; Jaigirdar, L.; Pham, W.; Kovtunov, K. V.; Koptyug, I. V.; Chekmenev, E. Y. Effects of Deuteration of 13C-Enriched Pholactate on Efficiency of Parahydrogen-Induced Polarization by Magnetic Field Cycling. *J. Phys. Chem. C* **2018**, *122* (43), 24740–24749. https://doi.org/10.1021/acs.jpcc.8b07365.

(149) Chekmenev, E. Y.; Hövener, J.; Norton, V. A.; Harris, K.; Batchelder, L. S.; Bhattacharya, P.; Ross, B. D.; Weitekamp, D. P. PASADENA Hyperpolarization of Succinic Acid for MRI and NMR Spectroscopy. *J. Am. Chem. Soc.* **2008**, *130* (13), 4212–4213. https://doi.org/10.1021/ja7101218.

(150) Olsson, L. E.; Chai, C.-M.; Axelsson, O.; Karlsson, M.; Golman, K.; Petersson, J. S. MR Coronary Angiography in Pigs with Intraarterial Injections of a Hyperpolarized 13C Substance. *Magn. Reson. Med.* **2006**, *55* (4), 731–737. https://doi.org/10.1002/mrm.20847.

(151) Reineri, F.; Cavallari, E.; Carrera, C.; Aime, S. Hydrogenative-PHIP Polarized Metabolites for Biological Studies. *Magn. Reson. Mater. Phys. Biol. Med.* **2021**, *34* (1), 25–47. https://doi.org/10.1007/s10334-020-00904-x.

(152) Butler, M. C.; Kervern, G.; Theis, T.; Ledbetter, M. P.; Ganssle, P. J.; Blanchard, J. W.; Budker, D.; Pines, A. Parahydrogen-Induced Polarization at Zero Magnetic Field. *J. Chem. Phys.* **2013**, *138* (23), 234201. https://doi.org/10.1063/1.4805062.

(153) Theis, T.; Ganssle, P.; Kervern, G.; Knappe, S.; Kitching, J.; Ledbetter, M. P.; Budker, D.; Pines, A. Parahydrogen-Enhanced Zero-Field Nuclear Magnetic Resonance. *Nat. Phys.* **2011**, *7* (7), 571–575. https://doi.org/10.1038/nphys1986.

(154) Emondts, M.; P. Colell, J. F.; Blümich, B.; M. Schleker, P. P. Polarization Transfer Efficiency in PHIP Experiments. *Phys. Chem. Chem. Phys.* **2017**, *19* (33), 21933–21937. https://doi.org/10.1039/C7CP04296E.

(155) Pravdivtsev, A. N.; Ivanov, K. L.; Yurkovskaya, A. V.; Vieth, H.-M.; Sagdeev, R. Z. Spontaneous Transfer of Para-Hydrogen Induced Polarization to 13C Spins in Symmetric Molecules1. *Dokl. Phys. Chem.* **2015**, *464* (2), 247–250. https://doi.org/10.1134/S0012501615100073.

(156) Eills, J.; Blanchard, J. W.; Wu, T.; Bengs, C.; Hollenbach, J.; Budker, D.; Levitt, M. H. Polarization Transfer via Field Sweeping in Parahydrogen-Enhanced Nuclear Magnetic Resonance. *J. Chem. Phys.* **2019**, *150* (17), 174202. https://doi.org/10.1063/1.5089486.

(157) Cavallari, E.; Carrera, C.; Aime, S.; Reineri, F. Studies to Enhance the Hyperpolarization Level in PHIP-SAH-Produced C13-Pyruvate. *J. Magn. Reson.* **2018**, *289*, 12–17. https://doi.org/10.1016/j.jmr.2018.01.019.

(158) Kuhn, L. T.; Bommerich, U.; Bargon, J. Transfer of Parahydrogen-Induced Hyperpolarization to 19F. *J. Phys. Chem. A* **2006**, *110* (10), 3521–3526. https://doi.org/10.1021/jp056219n.

(159) Stephan, M.; Kohlmann, O.; Niessen, H. G.; Eichhorn, A.; Bargon, J. 13C PHIP NMR Spectra and Polarization Transfer during the Homogeneous Hydrogenation of Alkynes with Parahydrogen. *Magn. Reson. Chem.* **2002**, *40* (2), 157–160. https://doi.org/10.1002/mrc.973.

(160) Jonischkeit, T.; Bommerich, U.; Stadler, J.; Woelk, K.; Niessen, H. G.; Bargon, J. Generating Long-Lasting H1 and C13 Hyperpolarization in Small Molecules with Parahydrogen-Induced Polarization. *J. Chem. Phys.* **2006**, *124* (20), 201109. https://doi.org/10.1063/1.2209235.

(161) Theis, T.; Truong, M. L.; Coffey, A. M.; Shchepin, R. V.; Waddell, K. W.; Shi, F.; Goodson, B. M.; Warren, W. S.; Chekmenev, E. Y. Microtesla SABRE Enables 10% Nitrogen-15 Nuclear Spin Polarization. *J. Am. Chem. Soc.* **2015**, *137* (4), 1404–1407. https://doi.org/10.1021/ja512242d.

(162) Truong, M. L.; Theis, T.; Coffey, A. M.; Shchepin, R. V.; Waddell, K. W.; Shi, F.; Goodson, B. M.; Warren, W. S.; Chekmenev, E. Y. 15N Hyperpolarization by Reversible Exchange Using SABRE-SHEATH. *J. Phys. Chem. C* **2015**, *119* (16), 8786–8797. https://doi.org/10.1021/acs.jpcc.5b01799.

(163) Pravdivtsev, A. N.; Ivanov, K. L.; Yurkovskaya, A. V.; Petrov, P. A.; Limbach, H.-H.; Kaptein, R.; Vieth, H.-M. Spin Polarization Transfer Mechanisms of SABRE: A Magnetic Field Dependent Study. *J. Magn. Reson.* **2015**, *261*, 73–82. https://doi.org/10.1016/j.jmr.2015.10.006.

(164) Zhivonitko, V. V.; Skovpin, I. V.; Koptyug, I. V. Strong 31P Nuclear Spin Hyperpolarization Produced via Reversible Chemical Interaction with Parahydrogen. *Chem. Commun.* **2015**, *51* (13), 2506–2509. https://doi.org/10.1039/C4CC08115C.

(165) Lindale, J. R.; Eriksson, S. L.; Tanner, C. P. N.; Zhou, Z.; Colell, J. F. P.; Zhang, G.; Bae, J.; Chekmenev, E. Y.; Theis, T.; Warren, W. S. Unveiling Coherently Driven Hyperpolarization Dynamics in Signal Amplification by Reversible Exchange. *Nat. Commun.* **2019**, *10* (1), 395. https://doi.org/10.1038/s41467-019-08298-8.

(166) Pravdivtsev, A. N.; Kempf, N.; Plaumann, M.; Bernarding, J.; Scheffler, K.; Hövener, J.-B.; Buckenmaier, K. Coherent Evolution of Signal Amplification by Reversible Exchange in Two Alternating Fields (Alt-SABRE). *ArXiv210709294 Phys.* **2021**.

(167) Dagys, L.; Bengs, C.; Levitt, M. H. Low-Frequency Excitation of Singlet–Triplet Transitions. Application to Nuclear Hyperpolarization. *J. Chem. Phys.* **2021**, *155* (15), 154201. https://doi.org/10.1063/5.0065863.

(168) Buckenmaier, K.; Rudolph, M.; Fehling, P.; Steffen, T.; Back, C.; Bernard, R.; Pohmann, R.; Bernarding, J.; Kleiner, R.; Koelle, D.; Plaumann, M.; Scheffler, K. Mutual Benefit Achieved by Combining Ultralow-Field Magnetic Resonance and Hyperpolarizing Techniques. *Rev. Sci. Instrum.* **2018**, *89* (12), 125103. https://doi.org/10.1063/1.5043369.

(169) Blanchard, J. W.; Ripka, B.; Suslick, B. A.; Gelevski, D.; Wu, T.; Münnemann, K.; Barskiy, D. A.; Budker, D. Towards Large-Scale Steady-State Enhanced Nuclear Magnetization with in Situ Detection. *Magn. Reson. Chem.* **2021**, 1–8. https://doi.org/10.1002/mrc.5161.

(170) Arunkumar, N.; Bucher, D. B.; Turner, M. J.; TomHon, P.; Glenn, D.; Lehmkuhl, S.; Lukin, M. D.; Park, H.; Rosen, M. S.; Theis, T.; Walsworth, R. L. Micron-Scale NV-NMR Spectroscopy with Signal Amplification by Reversible Exchange. *PRX Quantum* **2021**, *2* (1), 010305. https://doi.org/10.1103/PRXQuantum.2.010305.

(171) Blanchard, J. W.; Ledbetter, M. P.; Theis, T.; Butler, M. C.; Budker, D.; Pines, A. High-Resolution Zero-Field NMR J-Spectroscopy of Aromatic Compounds. *J. Am. Chem. Soc.* **2013**, *135* (9), 3607–3612. https://doi.org/10.1021/ja312239v.

(172) Blanchard, J. W.; Wu, T.; Eills, J.; Hu, Y.; Budker, D. Zero- to Ultralow-Field Nuclear Magnetic Resonance J-Spectroscopy with Commercial Atomic Magnetometers. *J. Magn. Reson.* **2020**, *314*, 106723. https://doi.org/10.1016/j.jmr.2020.106723.

(173) Burueva, D. B.; Eills, J.; Blanchard, J. W.; Garcon, A.; Picazo-Frutos, R.; Kovtunov, K. V.; Koptyug, I. V.; Budker, D. Chemical Reaction Monitoring Using Zero-Field Nuclear Magnetic Resonance Enables Study of Heterogeneous Samples in Metal Containers. *Angew. Chem. Int. Ed.* **2020**, *59* (39), 17026–17032. https://doi.org/10.1002/anie.202006266.

(174) Tayler, M. C. D.; Theis, T.; Sjolander, T. F.; Blanchard, J. W.; Kentner, A.; Pustelny, S.; Pines, A.; Budker, D. Invited Review Article: Instrumentation for Nuclear Magnetic Resonance in Zero and Ultralow Magnetic Field. *Rev. Sci. Instrum.* **2017**, *88* (9), 091101. https://doi.org/10.1063/1.5003347.

(175) Myers, W.; Slichter, D.; Hatridge, M.; Busch, S.; Mößle, M.; McDermott, R.; Trabesinger, A.; Clarke, J. Calculated Signal-to-Noise Ratio of MRI Detected with SQUIDs and Faraday Detectors in Fields from 10µT to 1.5T. *J. Magn. Reson.* **2007**, *186* (2), 182–192. https://doi.org/10.1016/j.jmr.2007.02.007.

(176) Theis, T.; Blanchard, J. W.; Butler, M. C.; Ledbetter, M. P.; Budker, D.; Pines, A. Chemical Analysis Using J-Coupling Multiplets in Zero-Field NMR. *Chem. Phys. Lett.* **2013**, *580*, 160–165. https://doi.org/10.1016/j.cplett.2013.06.042.

(177) Theis, T.; Ledbetter, M. P.; Kervern, G.; Blanchard, J. W.; Ganssle, P. J.; Butler, M. C.; Shin, H. D.; Budker, D.; Pines, A. Zero-Field NMR Enhanced by Parahydrogen in Reversible Exchange. *J. Am. Chem. Soc.* **2012**, *134* (9), 3987–3990. https://doi.org/10.1021/ja2112405.

(178) Lee, S.-J.; Jeong, K.; Shim, J. H.; Lee, H. J.; Min, S.; Chae, H.; Namgoong, S. K.; Kim, K. SQUID-Based Ultralow-Field MRI of a Hyperpolarized Material Using Signal Amplification by Reversible Exchange. *Sci. Rep.* **2019**, *9* (1), 12422. https://doi.org/10.1038/s41598-019-48827-5.

(179) Vesanen, P. T.; Nieminen, J. O.; Zevenhoven, K. C. J.; Dabek, J.; Parkkonen, L. T.; Zhdanov, A. V.; Luomahaara, J.; Hassel, J.; Penttilä, J.; Simola, J.; Ahonen, A. I.; Mäkelä, J. P.; Ilmoniemi, R. J. Hybrid Ultra-Low-Field MRI and Magnetoencephalography System Based on a Commercial Whole-Head Neuromagnetometer. *Magn. Reson. Med.* **2013**, *69* (6), 1795–1804. https://doi.org/10.1002/mrm.24413.

(180) Bucher, D. B.; Glenn, D. R.; Park, H.; Lukin, M. D.; Walsworth, R. L. Hyperpolarization-Enhanced NMR Spectroscopy with Femtomole Sensitivity Using Quantum Defects in Diamond. *Phys. Rev. X* **2020**, *10* (2), 021053. https://doi.org/10.1103/PhysRevX.10.021053.

(181) Zheng, H.; Xu, J.; Iwata, G. Z.; Lenz, T.; Michl, J.; Yavkin, B.; Nakamura, K.; Sumiya, H.; Ohshima, T.; Isoya, J.; Wrachtrup, J.; Wickenbrock, A.; Budker, D. Zero-Field Magnetometry Based on Nitrogen-Vacancy Ensembles in Diamond. *Phys. Rev. Appl.* **2019**, *11* (6), 064068. https://doi.org/10.1103/PhysRevApplied.11.064068.

(182) Kimmich, R. Chapter 1 Principle, Purpose and Pitfalls of Field-Cycling NMR Relaxometry. **2018**, 1–41. https://doi.org/10.1039/9781788012966-00001.

(183) Ivanov, K. L.; Pravdivtsev, A. N.; Yurkovskaya, A. V.; Vieth, H.-M.; Kaptein, R. The Role of Level Anti-Crossings in Nuclear Spin Hyperpolarization. *Prog.*

Nucl. Magn. Reson. Spectrosc. **2014**, *81*, 1–36. https://doi.org/10.1016/j.pnmrs.2014.06.001.

(184) Shchepin, R. V.; Barskiy, D. A.; Coffey, A. M.; Manzanera Esteve, I. V.; Chekmenev, E. Y. Efficient Synthesis of Molecular Precursors for Para-Hydrogen-Induced Polarization of Ethyl Acetate-1-13C and Beyond. *Angew. Chem. Int. Ed.* **2016**, *55* (20), 6071–6074. https://doi.org/10.1002/anie.201600521.

(185) Reineri, F.; Viale, A.; Dastrù, W.; Gobetto, R.; Aime, S. How to Design 13C Para-Hydrogen-Induced Polarization Experiments for MRI Applications. *Contrast Media Mol. Imaging* **2011**, *6* (2), 77–84. https://doi.org/10.1002/cmmi.407.

(186) Reineri, F.; Viale, A.; Ellena, S.; Alberti, D.; Boi, T.; Giovenzana, G. B.; Gobetto, R.; Premkumar, S. S. D.; Aime, S. 15N Magnetic Resonance Hyperpolarization via the Reaction of Parahydrogen with 15N-Propargylcholine. *J. Am. Chem. Soc.* **2012**, *134* (27), 11146–11152. https://doi.org/10.1021/ja209884h.

(187) Ellena, S.; Viale, A.; Gobetto, R.; Aime, S. Para-Hydrogen Induced Polarization of Si-29 NMR Resonances as a Potentially Useful Tool for Analytical Applications. *Magn. Reson. Chem.* **2012**, *50* (8), 529–533. https://doi.org/10.1002/mrc.3832.

(188) Eills, J.; Cavallari, E.; Carrera, C.; Budker, D.; Aime, S.; Reineri, F. Real-Time Nuclear Magnetic Resonance Detection of Fumarase Activity Using Parahydrogen-Hyperpolarized [1-13C]Fumarate. *J. Am. Chem. Soc.* **2019**, *141* (51), 20209–20214. https://doi.org/10.1021/jacs.9b10094.

(189) Ripka, B.; Eills, J.; Kouřilová, H.; Leutzsch, M.; H. Levitt, M.; Münnemann, K. Hyperpolarized Fumarate via Parahydrogen. *Chem. Commun.* **2018**, *54* (86), 12246–12249. https://doi.org/10.1039/C8CC06636A.

(190) A. Rodin, B.; Eills, J.; Picazo-Frutos, R.; F. Sheberstov, K.; Budker, D.; L. Ivanov, K. Constant-Adiabaticity Ultralow Magnetic Field Manipulations of Parahydrogen-Induced Polarization: Application to an AA'X Spin System. *Phys. Chem. Chem. Phys.* **2021**, *23* (12), 7125–7134. https://doi.org/10.1039/D0CP06581A.

(191) Reineri, F.; Santelia, D.; Gobetto, R.; Aime, S. Effect of Low and Zero Magnetic Field on the Hyperpolarization Lifetime in Parahydrogenated Perdeuterated Molecules. *J. Magn. Reson. San Diego Calif 1997* **2009**, *200* (1), 15–20. https://doi.org/10.1016/j.jmr.2009.05.009.

(192) Pokochueva, E. V.; Burueva, D. B.; Salnikov, O. G.; Koptyug, I. V. Heterogeneous Catalysis and Parahydrogen-Induced Polarization. *ChemPhysChem* **2021**, *22* (14), 1421–1440. https://doi.org/10.1002/cphc.202100153.

(193) Kovtunov, K. V.; Barskiy, D. A.; Shchepin, R. V.; Coffey, A. M.; Waddell, K. W.; Koptyug, I. V.; Chekmenev, E. Y. Demonstration of Heterogeneous Parahydrogen Induced Polarization Using Hyperpolarized Agent Migration from Dissolved Rh(I) Complex to Gas Phase. *Anal. Chem.* **2014**, *86* (13), 6192–6196. https://doi.org/10.1021/ac5013859.

(194) Kovtunov, K. V.; Zhivonitko, V. V.; Skovpin, I. V.; Barskiy, D. A.; Salnikov, O. G.; Koptyug, I. V. Toward Continuous Production of Catalyst-Free Hyperpolarized Fluids Based on Biphasic and Heterogeneous Hydrogenations with Parahydrogen. *J. Phys. Chem. C* **2013**, *117* (44), 22887–22893. https://doi.org/10.1021/jp407348r.

(195) Salnikov, O. G.; Kovtunov, K. V.; Koptyug, I. V. Production of Catalyst-Free Hyperpolarised Ethanol Aqueous Solution via Heterogeneous Hydrogenation with Parahydrogen. *Sci. Rep.* **2015**, *5* (1), 13930. https://doi.org/10.1038/srep13930.

(196) Salnikov, O. G.; Svyatova, A.; Kovtunova, L. M.; Chukanov, N. V.; Bukhtiyarov, V. I.; Kovtunov, K. V.; Chekmenev, E. Y.; Koptyug, I. V. Heterogeneous Parahydrogen-Induced Polarization of Diethyl Ether for Magnetic Resonance Imaging Applications. *Chem. – Eur. J.* **2021**, *27* (4), 1316–1322. https://doi.org/10.1002/chem.202003638.

(197) Du, Y.; Behera, R.; Maligal-Ganesh, R. V.; Chen, M.; Chekmenev, E. Y.; Huang, W.; Bowers, C. R. Cyclopropane Hydrogenation vs Isomerization over Pt and Pt–Sn Intermetallic Nanoparticle Catalysts: A Parahydrogen Spin-Labeling Study. *J. Phys. Chem. C* **2020**, *124* (15), 8304–8309. https://doi.org/10.1021/acs.jpcc.0c02493.

(198) Zhou, R.; Cheng, W.; Neal, L. M.; Zhao, E. W.; Ludden, K.; Hagelin-Weaver, H. E.; Bowers, C. R. Parahydrogen Enhanced NMR Reveals Correlations in Selective Hydrogenation of Triple Bonds over Supported Pt Catalyst. *Phys. Chem. Chem. Phys.* **2015**, *17* (39), 26121–26129. https://doi.org/10.1039/C5CP04223B.

(199) Burueva, D. B.; Kozinenko, V. P.; Sviyazov, S. V.; Kovtunova, L. M.; Bukhtiyarov, V. I.; Chekmenev, E. Y.; Salnikov, O. G.; Kovtunov, K. V.; Koptyug, I. V. Gas-Phase NMR of Hyperpolarized Propane with 1H-to-13C Polarization Transfer by PH-INEPT. *Appl. Magn. Reson.* **2021**. https://doi.org/10.1007/s00723-021-01377-4.

(200) Salnikov, O. G.; Nikolaou, P.; Ariyasingha, N. M.; Kovtunov, K. V.; Koptyug, I. V.; Chekmenev, E. Y. Clinical-Scale Batch-Mode Production of Hyperpolarized Propane Gas for MRI. *Anal. Chem.* **2019**, *91* (7), 4741–4746. https://doi.org/10.1021/acs.analchem.9b00259.

(201) Kovtunov, K. V.; Barskiy, D. A.; Coffey, A. M.; Truong, M. L.; Salnikov, O. G.; Khudorozhkov, A. K.; Inozemtseva, E. A.; Prosvirin, I. P.; Bukhtiyarov, V. I.; Waddell, K. W.; Chekmenev, E. Y.; Koptyug, I. V. High-Resolution 3D Proton MRI of Hyperpolarized Gas Enabled by Parahydrogen and Rh/TiO2 Heterogeneous Catalyst. *Chem. Weinh. Bergstr. Ger.* **2014**, *20* (37), 11636–11639. https://doi.org/10.1002/chem.201403604.

(202) Salnikov, O. G.; Kovtunov, K. V.; Nikolaou, P.; Kovtunova, L. M.; Bukhtiyarov, V. I.; Koptyug, I. V.; Chekmenev, E. Y. Heterogeneous Parahydrogen Pairwise Addition to Cyclopropane. *Chemphyschem Eur. J. Chem. Phys. Phys. Chem.* **2018**, *19* (20), 2621–2626. https://doi.org/10.1002/cphc.201800690.

(203) Burueva, D. B.; Kovtunov, K. V.; Bukhtiyarov, A. V.; Barskiy, D. A.; Prosvirin, I. P.; Mashkovsky, I. S.; Baeva, G. N.; Bukhtiyarov, V. I.; Stakheev, A. Yu.; Koptyug, I. V. Selective Single-Site Pd−In Hydrogenation Catalyst for Production of Enhanced Magnetic Resonance Signals Using Parahydrogen. *Chem. – Eur. J.* **2018**, *24* (11), 2547–2553. https://doi.org/10.1002/chem.201705644.

(204) Telkki, V.-V.; Zhivonitko, V. V.; Ahola, S.; Kovtunov, K. V.; Jokisaari, J.; Koptyug, I. V. Microfluidic Gas-Flow Imaging Utilizing Parahydrogen-Induced Polarization and Remote-Detection NMR. *Angew. Chem. Int. Ed.* **2010**, *49* (45), 8363–8366. https://doi.org/10.1002/anie.201002685.

(205) Telkki, V.-V.; Zhivonitko, V. V. Analysis of Remote Detection Travel Time Curves Measured from Microfluidic Channels. *J. Magn. Reson.* **2011**, *210* (2), 238–245. https://doi.org/10.1016/j.jmr.2011.03.011.

(206) Bouchard, L.-S.; Burt, S. R.; Anwar, M. S.; Kovtunov, K. V.; Koptyug, I. V.; Pines, A. NMR Imaging of Catalytic Hydrogenation in Microreactors with the Use of Para-Hydrogen. *Science* **2008**, *319* (5862), 442–445. https://doi.org/10.1126/science.1151787.

(207) Zhivonitko, V. V.; Telkki, V.-V.; Koptyug, I. V. Characterization of Microfluidic Gas Reactors Using Remote-Detection MRI and Parahydrogen-Induced Polarization. *Angew. Chem.* **2012**, *124* (32), 8178–8182. https://doi.org/10.1002/ange.201202967.

(208) Kovtunov, K. V.; Lebedev, D.; Svyatova, A.; Pokochueva, E. V.; Prosvirin, I. P.; Gerasimov, E. Y.; Bukhtiyarov, V. I.; Müller, C. R.; Fedorov, A.; Koptyug, I. V. Robust In Situ Magnetic Resonance Imaging of Heterogeneous Catalytic Hydrogenation with and without Hyperpolarization. *ChemCatChem* **2019**, *11* (3), 969–973. https://doi.org/10.1002/cctc.201801820.

(209) Svyatova, A.; S. Kononenko, E.; V. Kovtunov, K.; Lebedev, D.; Yu. Gerasimov, E.; V. Bukhtiyarov, A.; P. Prosvirin, I.; I. Bukhtiyarov, V.; R. Müller, C.; Fedorov, A.; V. Koptyug, I. Spatially Resolved NMR Spectroscopy of Heterogeneous Gas Phase Hydrogenation of 1,3-Butadiene with Para Hydrogen. *Catal. Sci. Technol.* **2020**, *10* (1), 99–104. https://doi.org/10.1039/C9CY02100K.

(210) Barskiy, D. A.; Kovtunov, K. V.; Gerasimov, E. Y.; Phipps, M. A.; Salnikov, O. G.; Coffey, A. M.; Kovtunova, L. M.; Prosvirin, I. P.; Bukhtiyarov, V. I.; Koptyug, I. V.; Chekmenev, E. Y. 2D Mapping of NMR Signal Enhancement and Relaxation for Heterogeneously Hyperpolarized Propane Gas. *J. Phys. Chem. C* **2017**, *121* (18), 10038–10046. https://doi.org/10.1021/acs.jpcc.7b02506.

(211) Ariyasingha, N. M.; Salnikov, O. G.; Kovtunov, K. V.; Kovtunova, L. M.; Bukhtiyarov, V. I.; Goodson, B. M.; Rosen, M. S.; Koptyug, I. V.; Gelovani, J. G.; Chekmenev, E. Y. Relaxation Dynamics of Nuclear Long-Lived Spin States in Propane and Propane-D6 Hyperpolarized by Parahydrogen. *J. Phys. Chem. C* **2019**, *123* (18), 11734–11744. https://doi.org/10.1021/acs.jpcc.9b01538.

(212) Barskiy, D. A.; Salnikov, O. G.; Romanov, A. S.; Feldman, M. A.; Coffey, A. M.; Kovtunov, K. V.; Koptyug, I. V.; Chekmenev, E. Y. NMR Spin-Lock Induced Crossing (SLIC) Dispersion and Long-Lived Spin States of Gaseous Propane at Low Magnetic Field (0.05T). *J. Magn. Reson.* **2017**, *276*, 78–85. https://doi.org/10.1016/j.jmr.2017.01.014.

(213) Ariyasingha, N. M.; Joalland, B.; Younes, H. R.; Salnikov, O. G.; Chukanov, N. V.; Kovtunov, K. V.; Kovtunova, L. M.; Bukhtiyarov, V. I.; Koptyug, I. V.; Gelovani, J. G.; Chekmenev, E. Y. Parahydrogen-Induced Polarization of Diethyl Ether Anesthetic. *Chem. – Eur. J.* **2020**, *26* (60), 13621–13626. https://doi.org/10.1002/chem.202002528.

(214) Zhao, E. W.; Maligal-Ganesh, R.; Xiao, C.; Goh, T.-W.; Qi, Z.; Pei, Y.; Hagelin-Weaver, H. E.; Huang, W.; Bowers, C. R. Silica-Encapsulated Pt-Sn Intermetallic Nanoparticles: A Robust Catalytic Platform for Parahydrogen-Induced Polarization of Gases and Liquids. *Angew. Chem.* **2017**, *129* (14), 3983–3987. https://doi.org/10.1002/ange.201701314.

(215) Zhao, E. W.; Xin, Y.; Hagelin-Weaver, H. E.; Bowers, C. R. Semihydrogenation of Propyne over Cerium Oxide Nanorods, Nanocubes, and Nano-Octahedra: Facet-Dependent Parahydrogen-Induced Polarization. *ChemCatChem* **2016**, *8* (13), 2197–2201. https://doi.org/10.1002/cctc.201600270.

(216) Barskiy, D. A.; Salnikov, O. G.; Kovtunov, K. V.; Koptyug, I. V. NMR Signal Enhancement for Hyperpolarized Fluids Continuously Generated in Hydrogenation Reactions with Parahydrogen. *J. Phys. Chem. A* **2015**, *119* (6), 996–1006. https://doi.org/10.1021/jp510572d.

(217) Sharma, R.; Bouchard, L.-S. Strongly Hyperpolarized Gas from Parahydrogen by Rational Design of Ligand-Capped Nanoparticles. *Sci. Rep.* **2012**, *2* (1), 277. https://doi.org/10.1038/srep00277.

(218) Kidd, B. E.; Gesiorski, J. L.; Gemeinhardt, M. E.; Shchepin, R. V.; Kovtunov, K. V.; Koptyug, I. V.; Chekmenev, E. Y.; Goodson, B. M. Facile Removal of Homogeneous SABRE Catalysts for Purifying Hyperpolarized Metronidazole, a Potential Hypoxia Sensor. *J. Phys. Chem. C* **2018**, *122* (29), 16848–16852. https://doi.org/10.1021/acs.jpcc.8b05758.

(219) Cavallari, E.; Carrera, C.; Di Matteo, G.; Bondar, O.; Aime, S.; Reineri, F. In-Vitro NMR Studies of Prostate Tumor Cell Metabolism by Means of Hyperpolarized [1-13C]Pyruvate Obtained Using the PHIP-SAH Method. *Front. Oncol.* **2020**, *10*, 497. https://doi.org/10.3389/fonc.2020.00497.

(220) Bondar, O.; Cavallari, E.; Carrera, C.; Aime, S.; Reineri, F. Effect of the Hydrogenation Solvent in the PHIP-SAH Hyperpolarization of [1-13C]Pyruvate. *ArXiv210801497 Phys.* **2021**. https://doi.org/10.13140/RG.2.2.13422.95046.

(221) Cavallari, E.; Carrera, C.; Aime, S.; Reineri, F. Metabolic Studies of Tumor Cells Using [1-13C] Pyruvate Hyperpolarized by Means of PHIP-Side Arm Hydrogenation. *Chemphyschem Eur. J. Chem.*

32

Phys. Phys. Chem. **2019**, *20* (2), 318–325. https://doi.org/10.1002/cphc.201800652.

(222) Cavallari, E.; Carrera, C.; Reineri, F. ParaHydrogen Hyperpolarized Substrates for Molecular Imaging Studies. *Isr. J. Chem.* **2017**, *57* (9), 833–842. https://doi.org/10.1002/ijch.201700030.

(223) Srour, M.; Hadjiali, S.; Brunnengräber, K.; Weidler, H.; Xu, Y.; Breitzke, H.; Gutmann, T.; Buntkowsky, G. A Novel Wilkinson's Type Silica Supported Polymer Catalyst: Insights from Solid-State NMR and Hyperpolarization Techniques. *J. Phys. Chem. C* **2021**, *125* (13), 7178–7187. https://doi.org/10.1021/acs.jpcc.1c00112.

(224) Pokochueva, E. V.; Kovtunov, K. V.; Salnikov, O. G.; Gemeinhardt, M. E.; Kovtunova, L. M.; Bukhtiyarov, V. I.; Chekmenev, E. Y.; Goodson, B. M.; Koptyug, I. V. Heterogeneous Hydrogenation of Phenylalkynes with Parahydrogen: Hyperpolarization, Reaction Selectivity, and Kinetics. *Phys. Chem. Chem. Phys.* **2019**, *21* (48), 26477–26482. https://doi.org/10.1039/C9CP02913C.

(225) Salnikov, O. G.; Chukanov, N. V.; Shchepin, R. V.; Manzanera Esteve, I. V.; Kovtunov, K. V.; Koptyug, I. V.; Chekmenev, E. Y. Parahydrogen-Induced Polarization of 1-13C-Acetates and 1-13C-Pyruvates Using Sidearm Hydrogenation of Vinyl, Allyl, and Propargyl Esters. *J. Phys. Chem. C* **2019**, *123* (20), 12827–12840. https://doi.org/10.1021/acs.jpcc.9b02041.

(226) McCormick, J.; Grunfeld, A. M.; Ertas, Y. N.; Biswas, A. N.; Marsh, K. L.; Wagner, S.; Glöggler, S.; Bouchard, L.-S. Aqueous Ligand-Stabilized Palladium Nanoparticle Catalysts for Parahydrogen-Induced 13C Hyperpolarization. *Anal. Chem.* **2017**, *89* (13), 7190–7194. https://doi.org/10.1021/acs.analchem.7b01363.

(227) Pei, Y.; Chen, M.; Zhong, X.; Yunpu Zhao, T.; Ferrer, M.-J.; V. Maligal-Ganesh, R.; Ma, T.; Zhang, B.; Qi, Z.; Zhou, L.; R. Bowers, C.; Liu, C.; Huang, W. Pairwise Semi-Hydrogenation of Alkyne to Cis - Alkene on Platinum-Tin Intermetallic Compounds. *Nanoscale* **2020**, *12* (15), 8519–8524. https://doi.org/10.1039/D0NR00920B.

(228) McCormick, J.; Korchak, S.; Mamone, S.; Ertas, Y.; Liu, Z.; Verlinsky, L.; Wagner, S.; Gloeggler, S.; Bouchard, L. Over 12% Polarization and 20 Minute Lifetime of 15N on Choline Derivative Utilizing Parahydrogen and Rh Nanocatalyst in Water. *Angew. Chem. Int. Ed. 0* (ja). https://doi.org/10.1002/anie.201804185.

(229) Kadlecek, S.; Shaghaghi, H.; Siddiqui, S.; Profka, H.; Pourfathi, M.; Rizi, R. The Effect of Exogenous Substrate Concentrations on True and Apparent Metabolism of Hyperpolarized Pyruvate in the Isolated Perfused Lung. *NMR Biomed.* **2014**, *27* (12), 1557–1570. https://doi.org/10.1002/nbm.3219.

(230) Eills, J.; Alonso-Valdesueiro, J.; Salazar Marcano, D. E.; Ferreira da Silva, J.; Alom, S.; Rees, G. J.; Hanna, J. V.; Carravetta, M.; Levitt, M. H. Preservation of Nuclear Spin Order by Precipitation. *ChemPhysChem*

2018, *19* (1), 40–44. https://doi.org/10.1002/cphc.201701189.

(231) Eills, J.; Hale, W.; Sharma, M.; Rossetto, M.; Levitt, M. H.; Utz, M. High-Resolution Nuclear Magnetic Resonance Spectroscopy with Picomole Sensitivity by Hyperpolarization on a Chip. *J. Am. Chem. Soc.* **2019**, *141* (25), 9955–9963. https://doi.org/10.1021/jacs.9b03507.

(232) Bordonali, L.; Nordin, N.; Fuhrer, E.; MacKinnon, N.; Korvink, J. G. Parahydrogen Based NMR Hyperpolarisation Goes Micro: An Alveolus for Small Molecule Chemosensing. *Lab. Chip* **2019**, *19* (3), 503–512. https://doi.org/10.1039/C8LC01259H.

(233) Ostrowska, S. J.; Rana, A.; Utz, M. Spatially Resolved Kinetic Model of Parahydrogen Induced Polarisation (PHIP) in a Microfluidic Chip. *ChemPhysChem* **2021**, *22* (19), 2004–2013. https://doi.org/10.1002/cphc.202100135.

(234) Eills, J.; Hale, W.; Utz, M. Synergies between Hyperpolarized NMR and Microfluidics: A Review. *Prog. Nucl. Magn. Reson. Spectrosc.* **2021**. https://doi.org/10.1016/j.pnmrs.2021.09.001.

(235) Suefke, M.; Lehmkuhl, S.; Liebisch, A.; Blümich, B.; Appelt, S. Para-Hydrogen Raser Delivers Sub-Millihertz Resolution in Nuclear Magnetic Resonance. *Nat. Phys.* **2017**, *13* (6), 568–572. https://doi.org/10.1038/nphys4076.

(236) Joalland, B.; Theis, T.; Appelt, S.; Chekmenev, E. Y. Background-Free Proton NMR Spectroscopy with Radiofrequency Amplification by Stimulated Emission Radiation. *Angew. Chem. Int. Ed. n/a* (n/a). https://doi.org/10.1002/anie.202108939.

(237) Gilles, H.; Monfort, Y.; Hamel, J. 3He Maser for Earth Magnetic Field Measurement. *Rev. Sci. Instrum.* **2003**, *74* (10), 4515–4520. https://doi.org/10.1063/1.1605494.

(238) Heil, W.; Gemmel, C.; Karpuk, S.; Sobolev, Y.; Tullney, K.; Allmendinger, F.; Schmidt, U.; Burghoff, M.; Kilian, W.; Knappe-Grüneberg, S.; Schnabel, A.; Seifert, F.; Trahms, L. Spin Clocks: Probing Fundamental Symmetries in Nature. *Ann. Phys.* **2013**, *525* (8–9), 539–549. https://doi.org/10.1002/andp.201300048.

(239) Chen, H.-Y.; Lee, Y.; Bowen, S.; Hilty, C. Spontaneous Emission of NMR Signals in Hyperpolarized Proton Spin Systems. *J. Magn. Reson. San Diego Calif 1997* **2011**, *208* (2), 204–209. https://doi.org/10.1016/j.jmr.2010.11.002.

(240) Iali, W.; Rayner, P. J.; Duckett, S. B. Using Parahydrogen to Hyperpolarize Amines, Amides, Carboxylic Acids, Alcohols, Phosphates, and Carbonates. *Sci. Adv.* **2018**, *4* (1), eaao6250. https://doi.org/10.1126/sciadv.aao6250.

(241) M. Richardson, P.; O. John, R.; J. Parrott, A.; J. Rayner, P.; Iali, W.; Nordon, A.; E. Halse, M.; B. Duckett, S. Quantification of Hyperpolarisation Efficiency in SABRE and SABRE-Relay Enhanced NMR Spectroscopy. *Phys. Chem. Chem. Phys.* **2018**, *20* (41), 26362–26371. https://doi.org/10.1039/C8CP05473H.

(242)   Knecht, S.; Barskiy, D. A.; Buntkowsky, G.; Ivanov,
K. L. Theoretical Description of Hyperpolarization
Formation in the SABRE-Relay Method. *J. Chem.
Phys.* **2020**, *153* (16), 164106.
https://doi.org/10.1063/5.0023308.

Table of Contents Figure: